NATIONAL AERONAUTICS AND SPACE ADMINISTRATION

Technical Report 32-1604

Five-Meter-Diameter Conical Furlable Antenna

JET PROPULSION LABORATORY
CALIFORNIA INSTITUTE OF TECHNOLOGY
PASADENA, CALIFORNIA

July 15, 1976

NATIONAL AERONAUTICS AND SPACE ADMINISTRATION

Technical Report 32-1604

Five-Meter-Diameter Conical Furlable Antenna

J. W. Fortenberry
R. E. Freeland
D. M. Moore

JET PROPULSION LABORATORY
CALIFORNIA INSTITUTE OF TECHNOLOGY
PASADENA, CALIFORNIA

July 15, 1976

Preface

The work described in this report was performed by the Applied Mechanics Division of the Jet Propulsion Laboratory.

Acknowledgment

The authors wish to express their thanks to the following individual members of JPL's Applied Mechanics Division: A. Wilson for conceptual development, design and mechanical testing and associated support equipment; F. Wolf for the thermal analysis; R. Norton for structural modeling and loads analysis; K. Gupta for dynamic model generation and derivation and application of the "dynamic element"; D. Kubly and A. McDougal for development, design and fabrication of the deployment mechanism; E. Nields for structural assembly of the antenna; and A. Knoell and W. Jensen for the application of composite materials to the antenna.

Our thanks also go to K. Woo and J. Hardy of JPL's Telecommunication Division for participation in the antenna design, supplying the line source feed, and performing the RF tests.

Finally, we would like to thank M. Sullivan of Harris Corp. for his effort in development of the silver-plated beryllium-copper mesh and D. Bangle of TEC Chemical for his help with the mesh surface degradation problem.

Contents

Tables

Figures

Abstract

The goals of the program reported here were two-fold: to demonstrate that a 5-meter-diameter, farlable, conical reflector antenna utilizing a line source feed can be fabricated utilizing composite materials and prove that the antenna can function mechanically and electrically as prototype flight hardware. The design, analysis, and testing of the antenna are described. An RF efficiency of 55% at 8.5 Ghz and a surface error of 0.64 mm rms were chosen as basic design requirements. Actual test measurements yielded an efficiency of 53% (49.77 dB gain) and a surface error of 0.61 mm rms. Atmospherically induced corrosion of the reflector mesh resulted in the RF performance degradation.

An assessment of the antenna as compared to the current state-of-the-art technology was made. This assessment included cost, surface accuracy and RF performance, structural and mechanical characteristics, and possible applications.

Five-Meter-Diameter Conical Furlable Antenna

I. Introduction

The most recent antenna development activity at JPL has been directed toward the conceptual development, mechanical design, fabrication, and testing of a 5-meter, flightlike, furlable, novel conical reflector antenna as differentiated from the classical parabolic reflector antenna. The antenna configuration selected for development uses a line source feed for radio frequency (RF) operation at X-band.

There are a number of space systems that either require or could benefit from the availability of large-aperture spacecraft-mounted antennas. For example, outer planet and planetary missions beyond 1980–1985 will require substantially increased communication capabilities. JPL studies of NASA mission models indicate that communicatio equirements associated with exploration of the outer anets require antennas up to 30 meters in diameter. Maximum size constraints for current and projected launch vehicles including the shuttle, limited to about 4 meters, necessitate the use of space-deployable or space-assembled antenna structures (Ref. 1). Since the projected deep space applications will be for unmanned missions, self-deployable antennas are needed.

For a number of years JPL has been investigating advanced concepts for antenna structures with respect to identification and delineation of the technology required for development of large furlable antennas in the 5- to 30-meter-diameter range. Achievements of the program have been reported in Refs. 1–16. The present report adds to this series. While the development of large, furlable, lightweight antennas throughout industry has been focused on parabolic antenna reflectors, JPL efforts have been directed toward new configurations involving singly curved, conical main reflectors (Refs. 17, 18). The primary impetus for this approach is the elimination of some of the basic mechanical problems associated with the double curvature of the paraboloid.

From 1970–1976, JPL developed three basic concepts—the Gregorian, the quadreflex and the line source feed—to the point of model fabrication and RF testing at frequencies up to X-band (Table 1).

Table 1. Summary of conical antenna development at JPL

Antenna concept	Model diameter, m	Ref.	RF efficiency, %
Gregorian (uses single large subreflector for two reflections of RF signal)	1.83 (five total)	6 11	≤1.0
	4.3	13	57.5
Quadreflex (uses two reflectors for four reflections of RF signal)	0.76 (nonfurlable)	13 11	60.0
	1.83		58.6
Line source feed (uses continuous feed along axis of conical reflector for single reflection of RF signal)	3.66 (nonfurlable)	9	66.0
	5.0 (described in this report)		53.0

Preliminary RF test results of the nonfurlable 3.66-m line source feed model were very promising; the mechanical configuration displayed advantages over the Gregorian and quadreflex antennas (Ref. 9). Therefore, the line source feed concept was chosen to demonstrate conical antenna performance, and a decision was made to design, fabricate, and test a 5-m-diameter furlable flightlike model.

II. Program Objectives

The general program objectives were to demonstrate that (1) a 5-m furlable conical antenna utilizing a line source feed could be fabricated utilizing composite materials, and (2) the antenna could function mechanically and electrically as a prototype flight hardware model. To meet these program objectives, a set of design objectives and criteria was established. These criteria were intended to be compatible with the anticipated requirements of missions ranging from long-term Earth orbits to outer-planet missions.

A minimum operating RF efficiency of 55% at X-band frequencies was chosen to be commensurate with deep space mission requirements. With efficiency and frequency as the starting point, design factors such as size, cost, surface error, RF blockage, weight, mechanical reliability, etc., were budgeted according to their participation in the overall RF performance. The specific design criteria used for the 5-m conical antenna development are shown in Table 2.

Table 2. Design criteria for 5-m conical antenna

Design condition	Criteria
Mechanical	
Deployed diameter	5 m
Deployed length	4 m
Furled diameter	1.5 m
Mass	37 kg
Surface tolerance	0.64 mm rms
Feed alignment	±0.2 cm (translation) 0.01 rad
Electrical	
Frequency	X-band (8.5 GHz)
Operating efficiency	55%
Gain	49.8 dB
Feed	Line source
Environmental	
Structural loads	Launch/deployment
Natural frequency	≥0.1 Hz deployed ≥12 Hz furled
Thermal	33 to 367 K

Functionally, the antenna was designed to perform both mechanically and electrically as prototype flight hardware. However, certain compromises, made to minimize fabrication costs, included many structural fittings and mechanisms that were heavier than state-of-the-art flight hardware because it was less costly to machine parts with ample wall thicknesses and reasonable tolerances. Additionally, no attempt was made to provide flight-quality hardware surface finishes for purposes of thermal control.

III. Antenna Description

The 5-m furlable antenna employs a conical main reflector and a line source feed located along the axis of the cone (Fig. 1). The conical reflector is made of a metallic mesh knitted from silver-plated beryllium copper, and is supported at its small diameter by the hub structure. It is also supported at its outside perimeter by a series of ribs, bowstrings, and spokes. The bowstrings are highly tensioned cables supported by the ribs and form the cone generatrices to control the tendency of the tensioned mesh to bulge inward toward the cone axis. The ribs emanate from the hub structure and react the tension in the bowstrings. The spokes, which run from the outer tip of each rib to the outer end of the line source feed, are adjustable and locate the outer periphery of the mesh reflector on the desired cone.

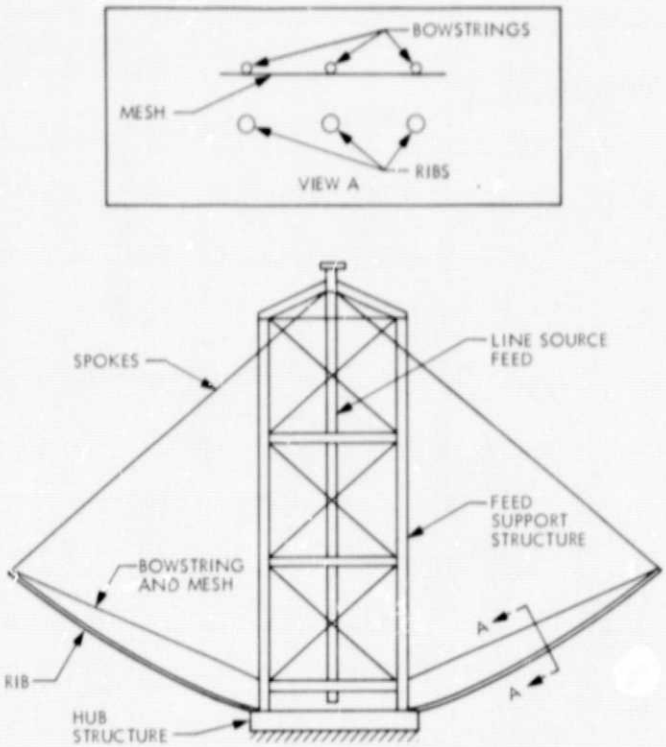

Fig. 1. Five-meter furlable antenna components

The basic geometry or angle of the conical reflector is controlled by the triangle formed by the spokes, bowstrings, and feed support structure located along the axis of the antenna. These structural elements were all constructed of Kevlar-49/epoxy composite, which minimizes the thermal distortion of this basic geometry. That is, although changes in the legs of the triangle will slightly alter the size of the antenna, the cone angle will remain constant.

The ribs, hinged from the hub structure, form a cage in the furled configuration to contain the mesh (Fig. 2). The ribs are furled and unfurled (deployed) by a four-bar linkage mechanism mounted on the hub structure. Front and side views of the deployed configuration are shown in Figs. 3 and 4.

IV. Design

A. Design Considerations

The mechanical factors that directly affect antenna RF performance for a given feed efficiency include:

(1) Reflector surface quality.

(2) Feed system mechanical alignment.

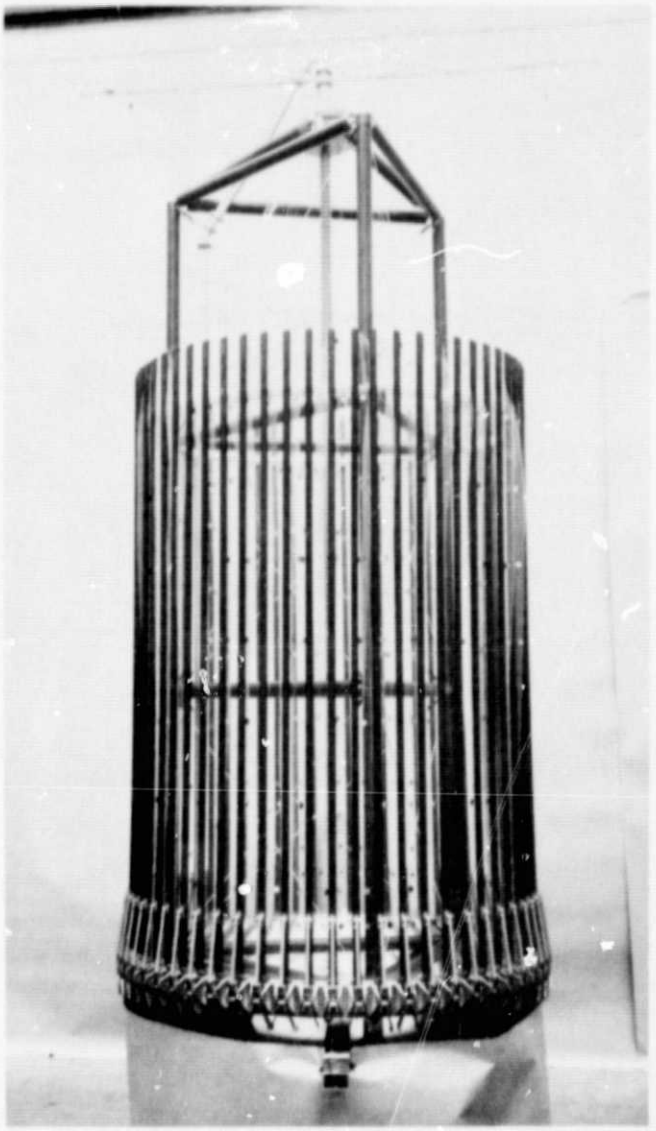

Fig. 2. Five-meter conical antenna in furled configuration

(3) RF transmission blockage by structure.

(4) Thermal stability.

The surface quality of furlable reflector antennas using a flexible mesh is a function of the support configuration, the tension field in the mesh, and characteristics of the mesh used. The critical parameters for the reflector that were determined from analysis include the number of ribs, the tension in bowstrings that support the mesh, and the circumferential and radial tension in the mesh.

The structural blockage and mechanical alignment of the antenna feed system are dependent on the mechanical

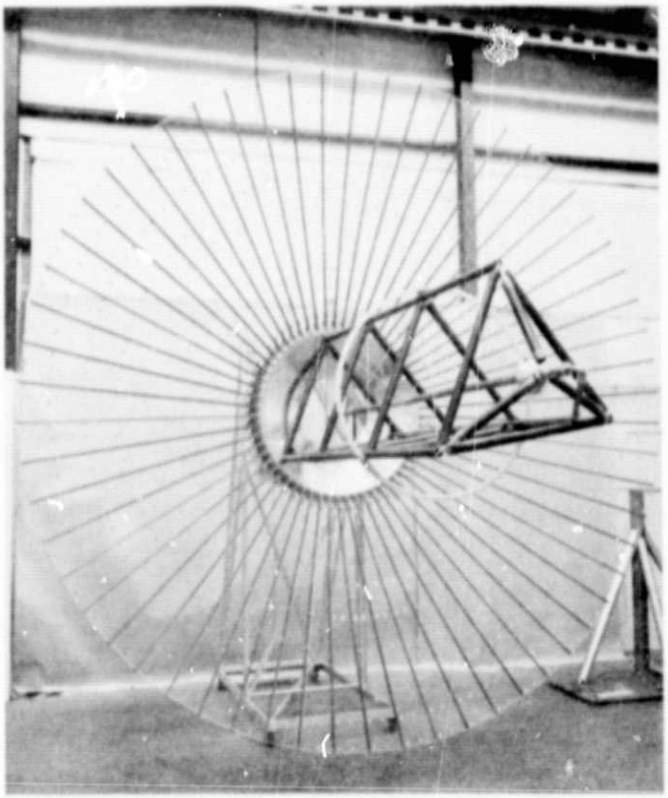

Fig. 3. Front view of deployed 5-meter conical antenna

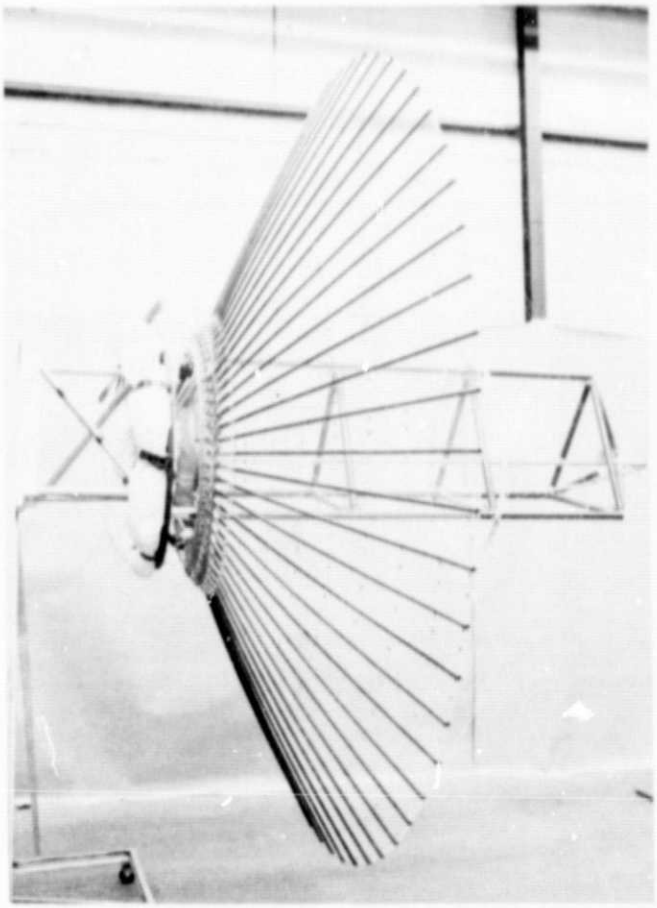

Fig. 4. Side view of deployed 5-meter conical antenna

configuration used and the RF transparency of the materials used. Two different structural configurations were evaluated for supporting the line source feed, and several different composite materials were considered.

The thermal stability of the entire antenna structure is dependent on the structural configuration, the service environment, and the thermal properties of the materials used for construction. For the design of the antenna, a worst-case thermal environment was assumed, i.e., a deep space trajectory away from the Sun, symmetric solar illumination, and nonsymmetric local heating from a radioisotope thermoelectric generator (RTG).

B. Reflector Surface Quality

For a given geometry, feed, and wavelength, the absolute gain of an antenna is limited by the diameter of the reflector and the rms surface deviation from the ideal surface (Ref. 19). Practical reflectors do not have perfect surfaces. The surface is a function of the number of ribs, bowstrings, and forward spokes that hold the mesh reflecting surface to a shape closely approximating the desired conical surface.

A membrane or mesh, stretched to form a conical shape, requires circumferential tension t to eliminate wrinkling and puckering and to provide for thermal expansion. However, this tension causes the mesh to bow inward toward the cone axis, resulting in a "lampshade" shape (Fig. 5 and Ref. 9).

Lampshading can be minimized by increasing the mesh radial tension T to very high levels. A tension ratio

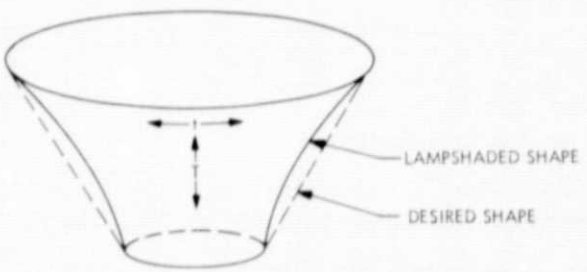

Fig. 5. The "lampshade" effect of mesh

T/t of 200 to 1 would be required to make the mesh surface sufficiently conical. However, T/t in excess of 4 to 1 produces wrinkles in the mesh.

To provide the high radial tension required, preloaded radial cables, called bowstrings, were used. The high tension load of the bowstrings is reacted by the ribs acting as a column. The bowstrings are placed on the inside surface of the mesh so that the tendency of the mesh to bow inward avoids the necessity of attaching the mesh to the bowstrings. The spoke tension and radial mesh tension are lumped together to produce an average radial tension used for calculating the average inward bowing of the mesh.

The minimum circumferential tension required was established by the requirement that the RF testing on the antenna was to be performed with the conical axis horizontal in a 1-g field. A conical mesh under the influence of gravity with its axis horizontal tends to assume the shape shown in Fig. 6.

That portion of the membrane above the horizontal axis tends to lampshade [illegible] the portion below tends to lampshade less, even [illegible] extent that it may assume the S-curve shown or hang completely below the desired cone surface. Since the spokes are inside the cone surface, they cannot control the membrane if it hangs outside the desired cone. Although the mesh could have been tied to the spokes, this was considered an undesirable complexity.

The minimum circumferential tension t in the mesh to avoid outward bulging of the mesh in a 1-g field in the horizontal position is given by (Ref. 20)

$$t_{min} = \frac{WD}{2}$$

where

t_{min} = minimum circumferential tension

W = mesh weight per unit area

D = antenna aperture

Based on a mesh weight of 0.36 N/m^2 (0.0075 lb/ft^2), the minimum t is 0.009 N/cm (0.005 lb/in.). To provide a conservative margin against the "sagging" phenomenon and to minimize wrinkles and thermal effects, a circumferential tension of 0.018 N/cm (0.010 lb/in.) was employed. A radial tension of 0.036 N/cm (0.020 lb/in.)

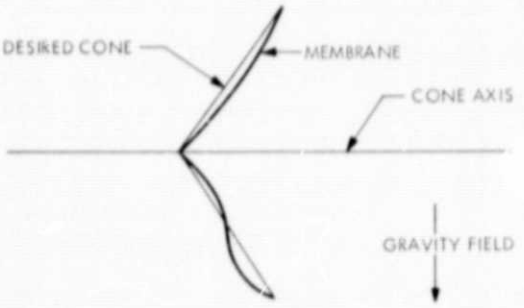

Fig. 6. Effect of gravity on conical mesh in horizontal position

was chosen empirically as providing the best compromise between the conflicting requirements of giving high radial tension and minimizing wrinkles in the mesh.

A FORTRAN computer program, COMESH (Ref. 20), was developed to calculate the surface shape of a [illegible]ched axisymmetric mesh bounded by two circular rings, concentric and perpendicular to a common axis. Inputs to the program include mesh weight per unit area, circumferential and radial tensions, number of bowstrings, bowstring tension, and the g-load parallel to the cone axis.

With the radial and circumferential tensions T and t and the cone dimensions fixed, COMESH was used to calculate the rms surface deviation due to lampshading as the number of bowstrings and bowstring tension were varied. The results of this parametric study are plotted in Fig. 7.

The use of bowstrings forces the mesh to form planar facets between adjacent bowstrings. These facets form an approximation of a true conical surface. This effect is additive to the surface deviation due to lampshading and is computed as

$$\text{rms}_{facet} = \frac{D}{8}\left[1-\cos\frac{180}{N}\right]\cos\theta$$

where

D = antenna aperture

N = number of bowstrings

θ = half angle of cone

The rms surface deviation due to faceting is also shown in Fig. 7.

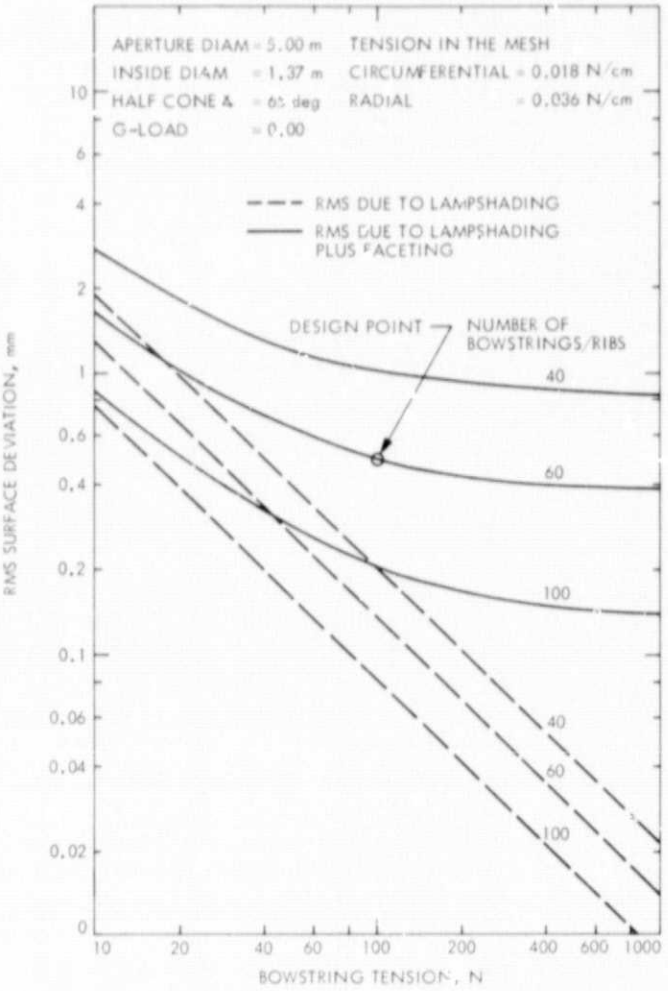

Fig. 7. RMS surface deviation as a function of bowstring parameters

The specified surface deviation for the antenna was 0.64 mm (0.025 in.) rms under the most adverse thermal environment. Experience with previous conical antennas indicated that fabrication and alignment errors were minor compared to the inherent geometric errors of lampshading and faceting. Therefore, 0.50 mm (0.020 in.) rms was allocated for the combined effects of lampshading and faceting. From Fig. 7 it can be seen that the minimum number of ribs required to attain 0.50 mm (0.020 in.) rms is approximately 53, with a bowstring load of 1000 N (223 lb). However, 60 ribs were chosen and the 0.50-mm (0.020-in.) rms surface deviation was achieved with a moderate, more acceptable, 100-N (22-lb) bowstring load.

C. Bowstrings, Ribs, Spokes

The bowstrings are tensioned cables whose main function is to shape the reflector mesh to the desired conical surface as closely as possible. In addition, the intersection of the bowstrings and spokes locates the outer periphery of the reflector and establishes the desired cone angle.

The primary design criterion for the bowstrings is the tension load when the antenna is fully deployed, since the bowstrings are slack in the furled (stowed) configuration. Additional design criteria were low cost, minimum weight, creep resistance, and a low coefficient of thermal expansion compatible with the rest of the structure. Urethane-impregnated Kevlar/49, an off-the-shelf material in fiber bundle form, satisfied these criteria.

The spokes originate at the top of the feed support structure and connect to each rib tip (Fig. 1). Adjusting the length of each spoke causes the respective rib to bow until the rib tip lies on the desired conical surface. Like the bowstrings, the spokes are slack in the stowed condition and the design loading criterion occurs in the deployed configuration. An additional requirement is that the spokes be as small and as RF-transparent as possible since they lie directly in the microwave path of the antenna.

The ribs are tubular members that react the tensile loads of the bowstrings and spokes in the deployed configuration. The bowstring load puts compression in the rib plus a small amount of bending due to eccentricity; the spoke load puts bending on the rib plus a small axial compression component.

In the stowed condition, corresponding to the launch configuration, the ribs are folded and form a cage that contains the mesh. The most severe stress in the ribs during the service environment is due to lateral bending induced by the vibratory launch loads. Therefore, the ribs were designed for launch and are stronger and stiffer than required for the deployed condition. This resulted in a design that was somewhat sensitive to thermally induced length changes of the ribs.

For thermal insensitivity, ideal rib stiffness would be designed for the deployed condition. Such design would permit elastic buckling due to the bowstring and spoke loads. Any thermally induced changes in rib length would be absorbed in the rib by a change in its bowed shape rather than an increase in the rib axial load. Because the launch environment precluded this design goal, thermal effects had to be considered.

A parametric study was made of various diameters, wall thicknesses, and materials for the ribs. Materials con-

sidered were aluminum, fiberglass, Kevlar/49 and graphite. The material selected was a high modulus graphite epoxy that had the greatest stiffness and lightest weight for a given diameter and wall thickness. In addition, the material closely matched the coefficient of thermal expansion of the Kevlar/49 bowstrings and spokes and therefore minimized thermal distortions. The final rib chosen had an internal diameter of 2.0 cm (0.8 in.) and a wall of 0.064 cm (0.025 in.).

The primary shortcomings of the graphite epoxy were greater cost, limited fabrication experience, and uncertain quality control. Because of the variation in quality, all the ribs received were tested at conditions more severe than those experienced on deployment. While in deployment, the spoke and bowstring loads were approximately 8.9 N (2-lb) and 133 N (30-lb), respectively. This loading produced a lateral bending deflection of about 2.3 cm (0.9 in.) in the rib. Each rib was tested with a 13.3-N (3.0-lb) spoke load and 267.0-N (60-lb) bowstring load in a fixture that simulated actual rib loading. Under these conditions, the rib deflection was about 3.56 cm (1.4 in.) (Fig. 8). Approximately 2% of the ribs failed under these testing conditions.

During initial rms measurements it was observed that rib bending led to deflections in excess of 5.1 cm (2 in.). In the process of furling and unfurling the antenna, three ribs failed. These ribs were replaced and bowstring loads were reduced to limit the deflection to 2.5 cm (1.0 in.). Rib deflection was chosen as the measure of spoke or bowstring loads. During months of subsequent operation and several deployments, no further failure occurred, showing that 2.5-cm (1.0-in.) rib deflection was an acceptable configuration.

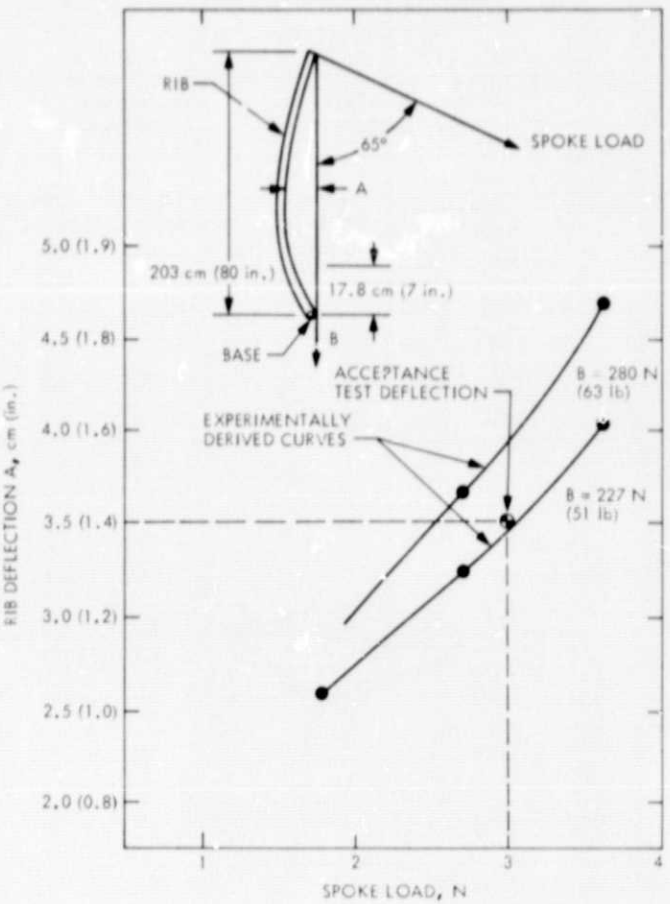

Fig. 8. Deflection/acceptance test criteria for graphite epoxy ribs

D. Feed Support

The main function of the feed support structure is to position and support the line feed along the axis of the conical reflector. It is also the backbone of the antenna; all other structural elements are attached to it. Launch environment loads imposed by the ribs and the line feed and the minimization of RF blockage are the primary design criteria.

The requirement of minimum RF blockage exerted the greatest influence on the feed support configuration (Ref. 15). The feed support is in the RF path from the line feed to the conical reflector. In addition, the closer an object is to the line feed, the larger the shadow (blockage) cast by that object on the reflector. Therefore, the feed support structure must be located as far from the feed as possible, but is limited by the additional constraint that the furled diameter be no greater than 1.5 m (59 in.)

Two types of feed support structures were initially considered; an open truss or space frame structure and a conical shell structure. Study of the two types showed that the anticipated RF blockage for the two structures was about the same. However, an increase in feed support diameter resulted in less blockage for the open truss design than for the shell design (Table 3). This was of importance since the concept under development was being considered for extrapolation to larger antennas.

The feed structure chosen was therefore a triangulated space frame consisting of three main longitudinal stringers, transverse members, and tensioned diagonals (Fig. 9). Epoxy-impregnated Kevlar-49 was chosen as the material because of low thermal expansion coefficient. The tubes have an inside diameter of 5.1 cm (2 in.) and a wall 0.635

Table 3. Comparison of RF blockage for two types of feed support structures

Antenna diameter, m (ft)	Conical membrane feed support			Space frame feed support		
	Average cone wall thickness, mm	(in.)	Cone blockage, dB	Truss main tube wall, mm	(in.)	Truss blockage, dB
5 (16.4)	0.635	(0.025)	0.5	0.51	(0.020)	0.5
10 (32.8)	1.02	(0.040)	>0.7	0.51	(0.020)	0.6
15 (49.2)	1.32	(0.052)	>1.0	0.64	(0.025)	0.7
20 (65.6)	1.60	(0.063)	>1.5	0.89	(0.035)	0.9

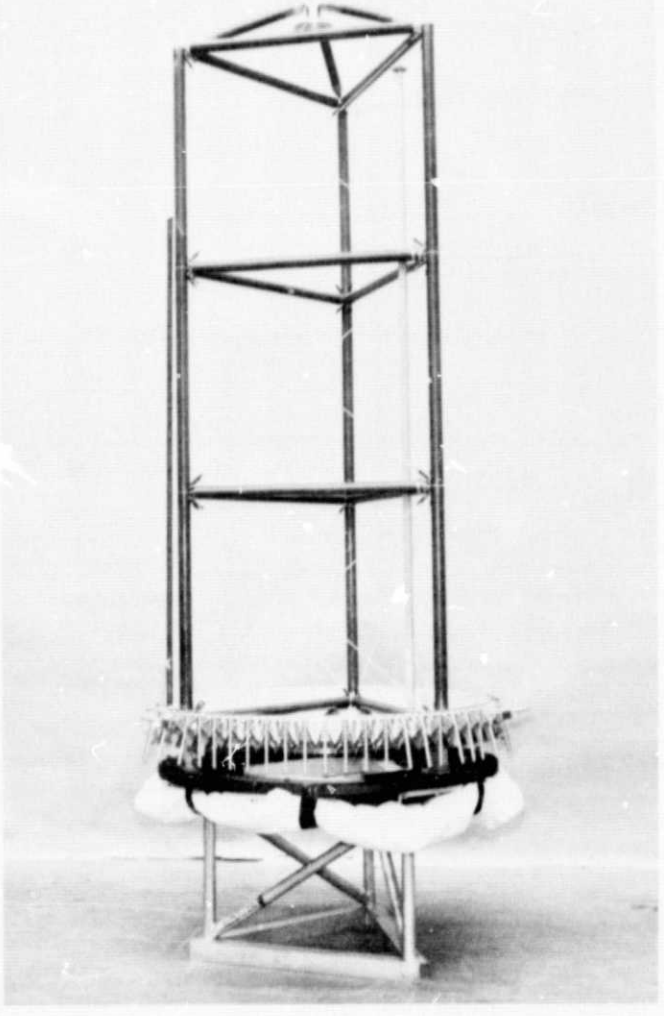

Fig. 9. Feed support structure

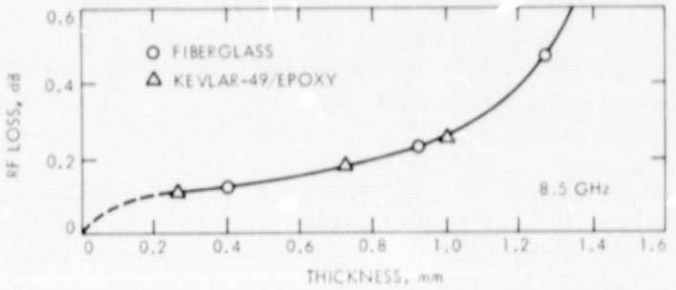

Fig. 10. RF loss vs thickness for fiberglass and Kevlar-49/epoxy

mm (0.025 in.) thick. Electrical considerations also played a determining role. Testing indicated that RF losses through Kevlar-49/epoxy were small and equal to those of fiberglass, another candidate material (Fig. 10). Because of its greater stiffness, Kevlar-49/epoxy was preferred for the local buckling critical stringers and transverse members. The resulting thinner members further enhanced RF performance.

Because of the variation in quality in the Kevlar-49/epoxy composite, all of the tubes used in the feed support were qualified by testing at 150% of design compressive load. Although the test screening was done without eccentric loading, it was judged adequate for detection of major flaws.

The square bays formed by the stringers and cross members were stabilized with diagonal tension rods 4 mm (0.157 in.) in diameter. The rods were made of fiberglass and were preloaded in tension by turnbuckles at each corner of the bay. Using the tensioned rods was dependent on devising a method of fastening the rod to the threaded coupling of the turnbuckle (Fig. 11, 12). The method used consisted of slitting the end of the rod and cementing a fiberglass wedge in the slit. This wedge then

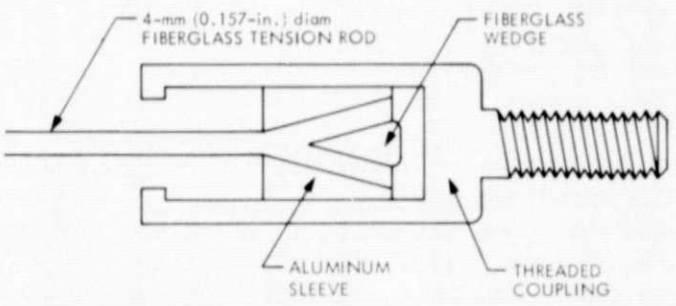

Fig. 11. Method of attaching tension rod diagonals to turnbuckle coupling

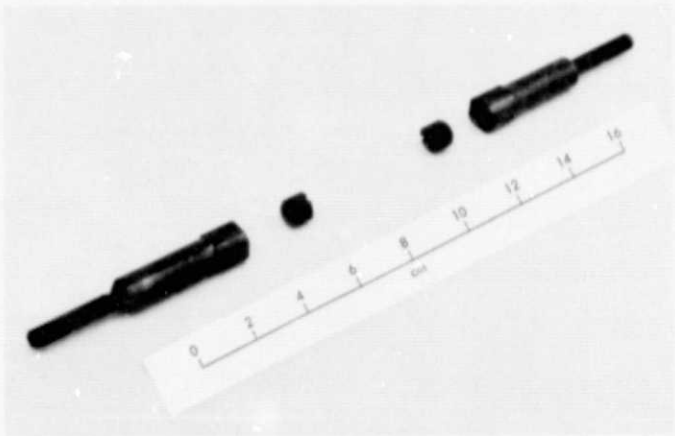

Fig. 12. Threaded couplings and aluminum sleeves

bears against a similar internal shape in an aluminum sleeve when load is applied.

The total RF blockage of the feed support was calculated to be 0.6 dB, based on the work in Ref. 15 and on estimated additional losses due to metal assembly hardware and thick sections used at load concentration points.

E. Hub Structure

The following components are mounted on and supported from the hub structure:

Inboard end of ribs.

Inboard end of bowstrings.

Deployment mechanism.

Inboard edge of mesh reflector.

In the stowed condition, the ribs are hinged at the hub and folded parallel to the antenna boresight. This configuration establishes the outside diameter of the hub, which is approximately equal to the maximum furled diameter of the antenna. The hub structure is supported at the same three points as the feed support structure so that the feed support structure loads are not fed through the hub structure, but directly to the supporting structure (spacecraft).

The critical loading condition for the hub structure results from inertial loading of the ribs, the deployment mechanism, and the hub structure itself and is produced by the vibratory launch environment. These loads are distributed uniformly around the periphery of the hub. Since the ring is supported at three discrete points, the hub structure will not be subjected to bending and torsion as a result of feed support structure loading. Thus, the hub structure takes the form of a circular ring girder of closed rectangular cross section (Figs. 13–15).

The hub structure was constructed entirely of aluminum as composite materials did not show any specific advantage for this particular piece of hardware. All gauges are heavier than required structurally to facilitate fabrication. A flight structure could be made considerably lighter. Because the structure is buckling critical, magnesium could be substituted for aluminum with substantial weight savings.

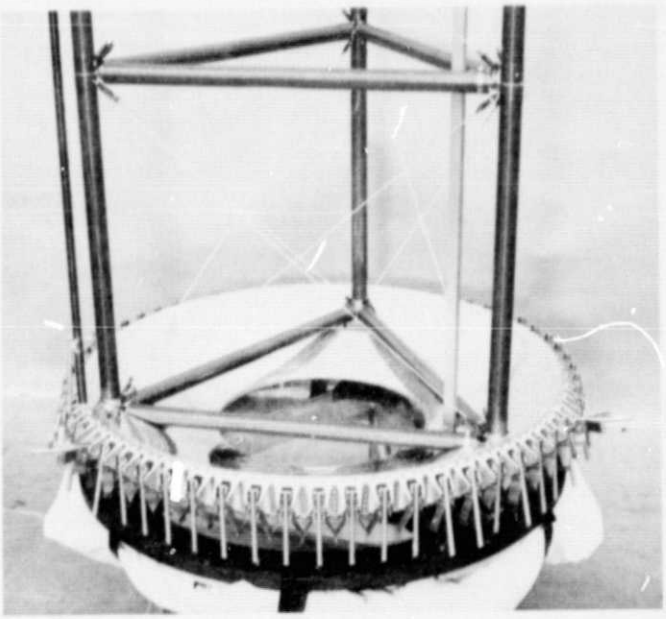

Fig. 13. Overall view of feed structure/hub interface

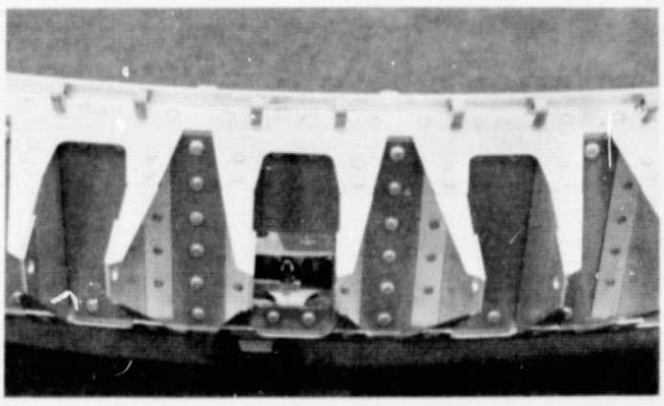

Fig. 14. Close-up of hub structure ring girder detail

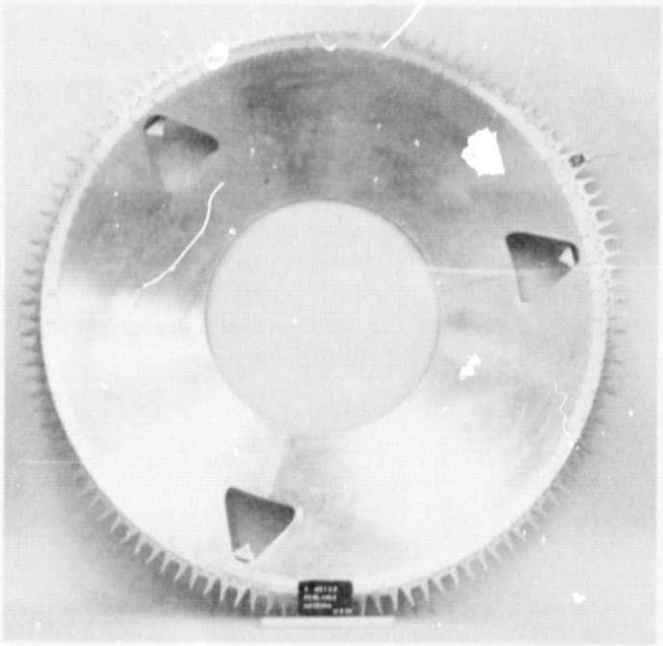

Fig. 15. Top view of hub ring girder

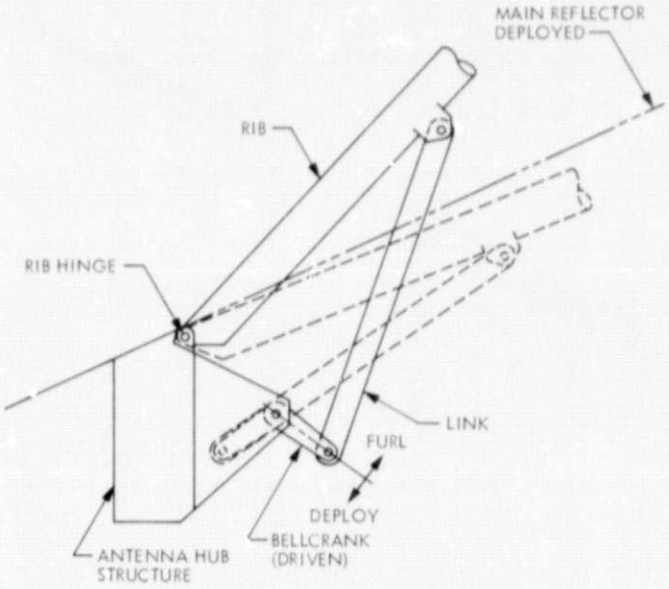

Fig. 16a. Schematic diagram of rib deployment (partially deployed — solid lines; fully deployed — dashed lines)

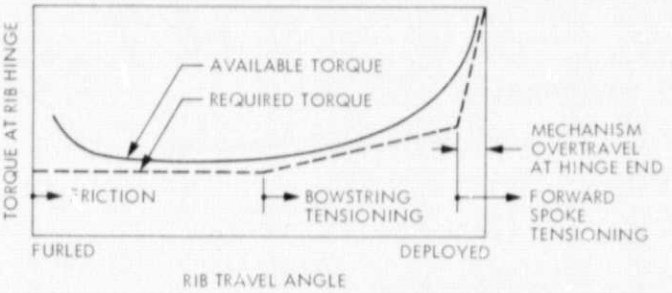

Fig. 16b. Deployment torque requirement compared to actuator torque available

F. Deployment Mechanism

The main function of the deployment mechanism is to move the ribs from the furled (stowed) position to the deployed (open) position and lock them in the deployed configuration.

The quasistatic loads, which the mechanism must overcome to effect deployment, are friction and tension in the bowstrings, spokes, and mesh. The hinge end of the rib must be moved somewhat past that position which places the rib parallel to the reflecting surface. The angle by which the travel of the hinge end of the rib exceeds the nominal travel requirement is called hinge end slope. This additional travel determines the tension in the forward spokes and the amount of rib bowing.

The mechanism designed to fulfill these requirements is shown schematically in Fig. 16a. It is a four-bar linkage mechanism with the rib, link, bellcrank, and antenna hub structure forming the four elements of the mechanism. Driving the bell crank causes the rib to rotate about its hinge axis. With the rib fully deployed, the bellcrank and link are in line, producing an over-center action which locks the rib in the deployed position.

The four-bar linkage is actuated by an electric motor and drive cable that produces an available torque at the rib hinge-line which is nearly ideal when compared to the friction and tension requirements (Fig. 16b). A reversible actuator was chosen to allow furling of the ribs as well as deployment. Twelve of the 60 ribs are driven from the single electric motor by means of a system of cables, pulleys, and pushrods linked to the bellcrank. The remaining 48 ribs are slaved to the motion of the 12 master ribs by means of blade-type flexures (Figs. 17 and 18). Deployment is typically accomplished in approximately 30 sec.

G. Mesh Development

The Jet Propulsion Laboratory and Harris Corporation collaborated in the development of an advanced-state-of-the-art mesh for application to this and future spacecraft antenna reflecting surfaces. The mesh is knitted from a

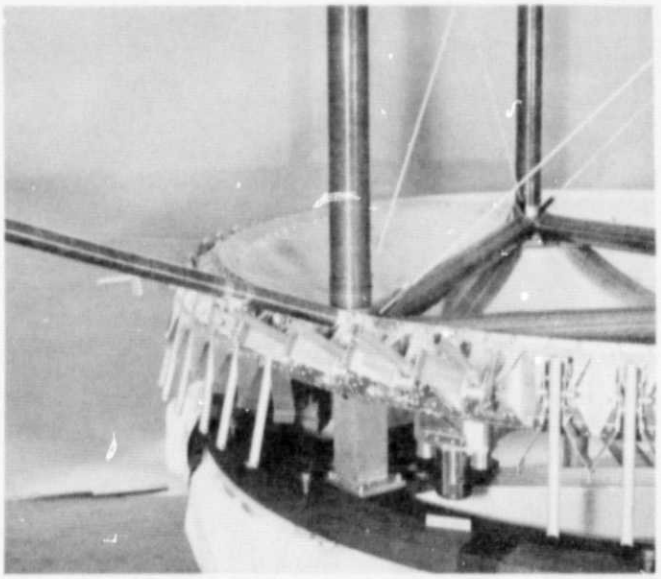

Fig. 17. Typical deployment link attachment to rib

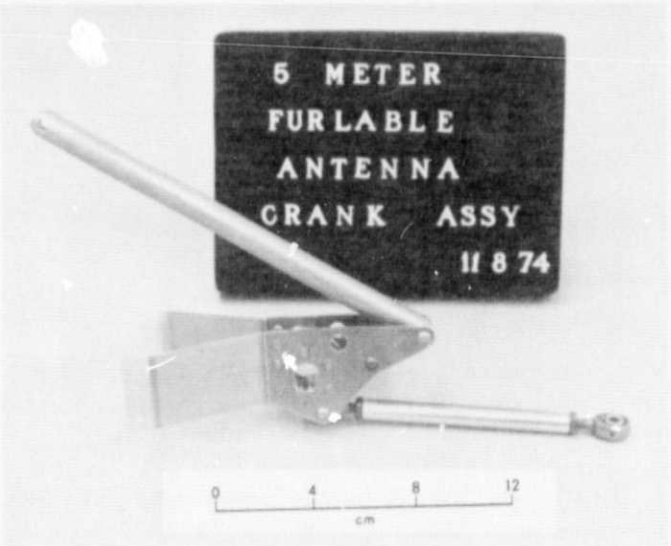

Fig. 18. View of link, bellcrank, push rod assembly

silver-plated beryllium copper wire. The distinctive features of this new material are discussed below as compared to the current state-of-the-art knitted mesh material (Refs. 9 and 21).

The desirable properties of an RF reflecting mesh can be enumerated as follows:

(1) Low cost.

(2) High RF reflectivity.

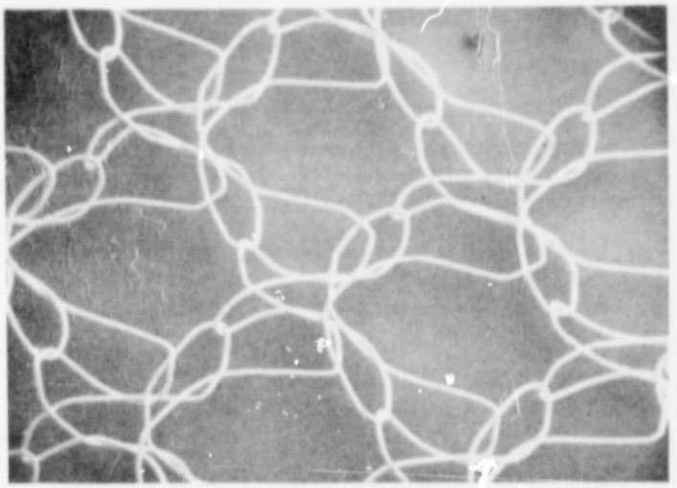

Fig 19. Silver-plated beryllium copper wire mesh (17× magnification)

(3) Corrosion resistance.

(4) Low weight.

(5) Low absorptivity/emissivity.

(6) Run, snag, wrinkle resistance.

(7) Biaxial compliance.

(8) High strength, puncture resistance.

(9) Low creep.

(10) Radiation resistance.

Many of these properties were optimized by selection of the proper material and fabrication technique.

The material is knitted from monafilament silver-plated beryllium copper wire. The knit pattern is a two-bar, half-set, warp knit fabric with diamond-shaped openings (Figs. 19 and 20). The pattern is more formally described by the knitting industry as:

Front bar: /1-0/1-2/2-3/2-1/

Back bar: /2-3/2-1/1-0/1-2/

The opening size is approximately 5 openings/cm, measured on the diagonal with the material stretched taut.

The beryllium copper wire is plated with 99.9% pure silver rather than gold to keep the mesh at a relatively low temperature. The silver produces a coating that is 4% by weight. This corresponds to a silver cladding nominal thickness of 0.00038 mm (0.000015 in.). Silver has a solar

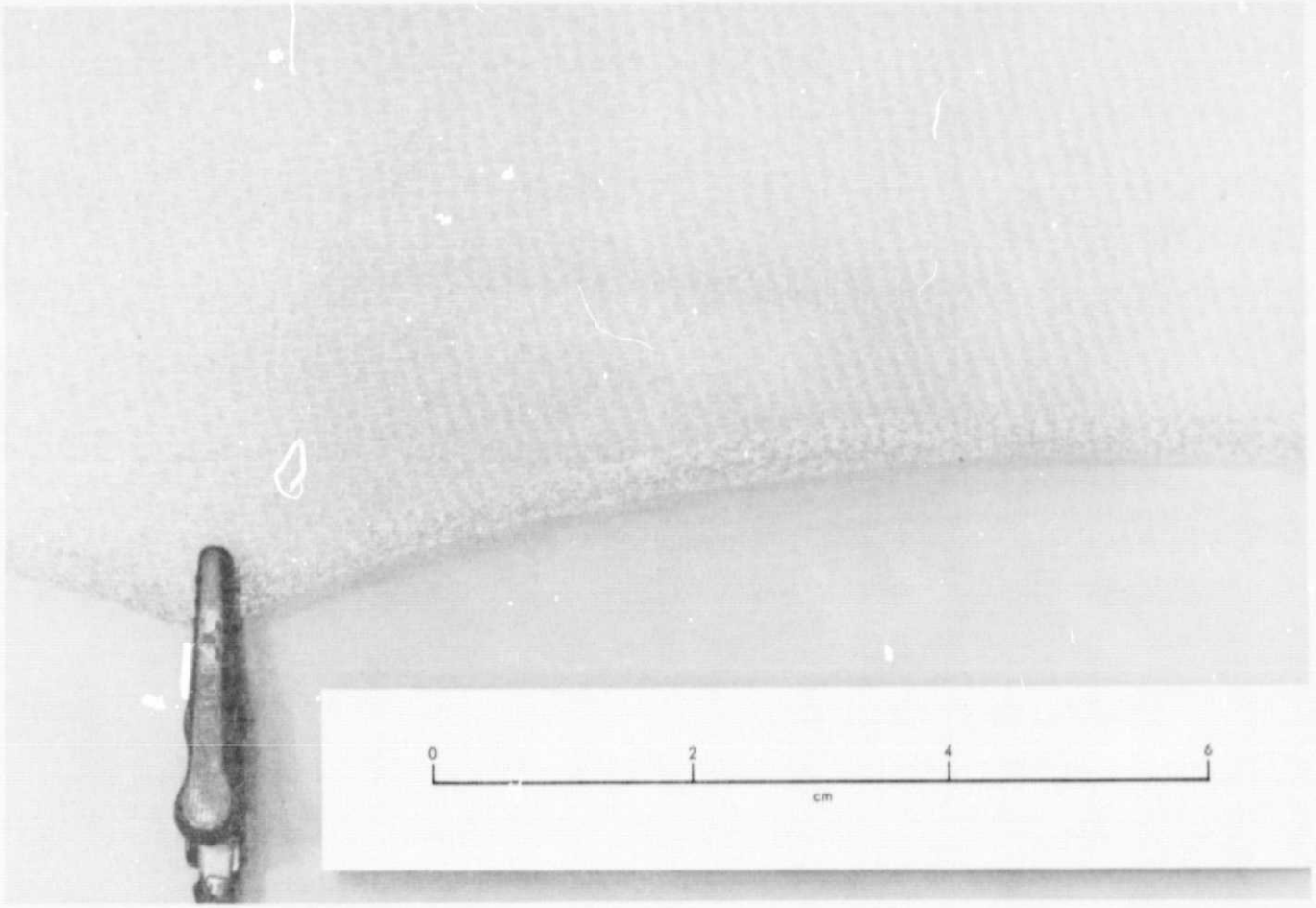

Fig. 20. Overall view of mesh knit pattern

absorptivity/emissivity ratio which results in a mesh temperature of 400 K (260°F) in Earth orbit. Gold on the other hand has a high absorptivity/emissivity ratio which would yield a mesh temperature as high as 473 K (392°F).

The wire core is 30% hard CDA alloy No. 172 with a composition of 97.9% Cu, 1.9% Be, 0.2% Co. The finished wire diameter is 0.038 mm (0.0015 in.). The weight of the silver-plated beryllium copper mesh is 0.36 N/m^2 (0.0075 lb/ft^2). The weight of the gold-plated chromel-R mesh is 0.72 N/m^2 (0.015 lb/ft^2). Therefore, the silver-plated wire represents a 50% weight saving for the main reflector mesh.

The cost of the silver-plated beryllium-copper-finished mesh is approximately \$430/m^2 (\$40/ft^2); the cost of the gold-plated chromel-R-finished mesh was about \$645/m^2 (\$60/ft^2). The cost of the beryllium copper wire used for knitting is considerably less than the cost of the chromel-R wire, and also the beryllium copper wire is preplated with silver prior to the knitting operation; the mesh knitted from chromel-R wire is gold-plated after knitting.

The RF reflectivity of a knitted mesh material depends on a number of factors. One of these factors, "geometric reflectivity," is described by the gauge of the mesh (yarn spacing) and the yarn diameter. For high reflectivity, the mesh opening size must be a small fraction of the RF wavelength at the operating frequency and the yarn diameter must be small compared to the mesh gauge. For operation at X-band (8.448 GHz, λ = 35 mm), mesh materials with an opening size of approximately 2 mm (0.08 in.) have performed well.

Given the proper geometry, low dc electrical resistance of the mesh is indicative of high RF reflectivity. Low resistivity depends on low resistance along the mesh conductors and low contact resistance at conductor junctions.

The beryllium copper wire core provides the low electrical resistance along the length of the wire, while the silver plating provides low contact resistance at wire junctions and enhances conduction along the wire.

The initial RF reflectivity of the mesh was measured by placing small samples of the mesh material in a waveguide. The results were good. Average RF reflectivity losses were 0.02, 0.04, and 0.07 dB for the 0-, 45-, and 90-deg positions, respectively. These losses compare favorably to the 0.03-, 0.03-, and 0.05-dB losses reported in Ref. 21 for the gold-plated chromel-R used on the 3.66-m antenna.

As a result of initial RF system tests of the whole antenna, it was found that the mesh surface RF reflectivity had degraded. This degradation was proportional to the time of exposure to the atmosphere. Further examination of the silver-coated beryllium copper wire indicated surface changes. Electrical resistance measurements showed decreased surface conductivity. Waveguide tests showed that the surface loss, less than 0.1 dB when new, was in excess of 2.5 dB in some cases.

Atmospheric corrosion of the mesh was found to be the cause of the RF degradation. The commercial corrosion-inhibiting coating, Tarnaban, applied to the silver-coated mesh after knitting, at the time of fabrication, was found to be ineffectual in preventing corrosion, since the RF reflectivity of the treated mesh was found to degrade unacceptably after exposure to an industrial atmosphere for a relatively short period of time. It must be noted that the gold-plated chromel-R mesh previously used (Ref. 9) was, on the contrary, virtually free from RF performance degradation due to atmospheric corrosion. To resolve the corrosion problem, several 2-in-diameter samples were taken from the antenna mesh. These samples were cleaned and treated with a variety of surface conditioners. Several treatments were effective in reducing the RF loss to approximately 0.1 dB. A dilute phosphoric acid was selected as a practical but temporary fix. It was found that after about four days of atmospheric exposure, mesh treated with this solution did not have losses of more than an acceptable 0.2 dB when measured in waveguide tests.

Alternative solutions involving gold plating achieved the same result in reducing RF loss but were estimated to be more costly in time and money, and would have defeated the reason for using silver in the first place. It should be noted that for an actual spacecraft application, the antenna would be in a vacuum and the cause of atmospheric degradation would disappear. However, the stability of the RF reflectivity of this new silver-coated mesh remains an open question that requires additional research.

V. Structural Analysis

The structural analysis accomplished in support of the design of the antenna was in two categories: (1) structural loads for member sizing and (2) dynamic modeling for structural/autopilot interaction. The analysis used to determine member loads and sizes was based on expected launch loads and utilized a finite element model of the antenna structure in the furled (boost) configuration (Fig. 21). Another analysis was done for the antenna structure in the cruise configuration in order to develop a mathematical model compatible for structural/autopilot interaction studies of potential applications (Fig. 22).

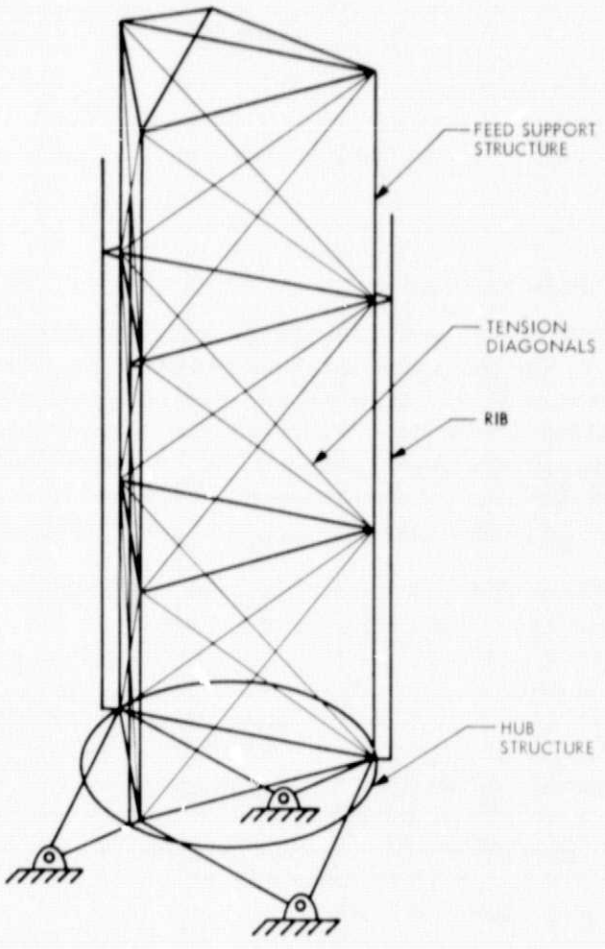

Fig. 21. Finite element model of 5-meter conical antenna in furled configuration

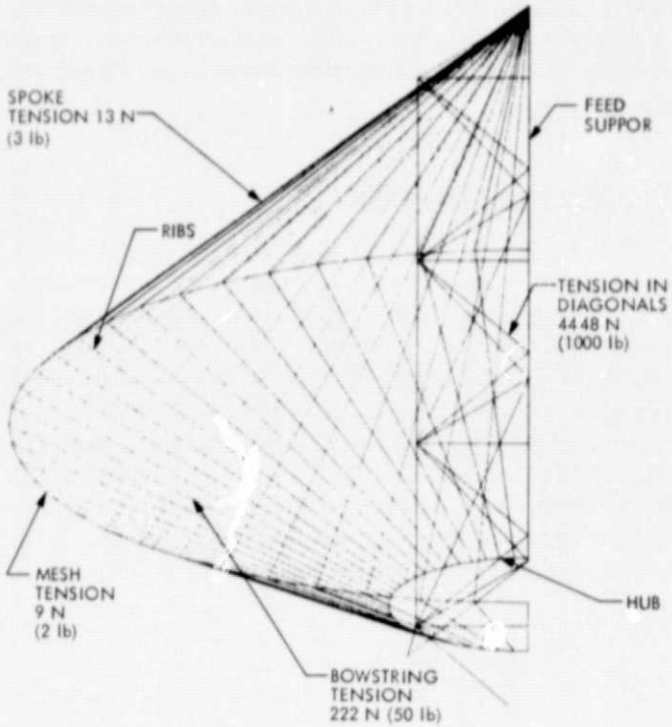

Fig. 22. Finite element model of 5-meter conical antenna in deployed configuration

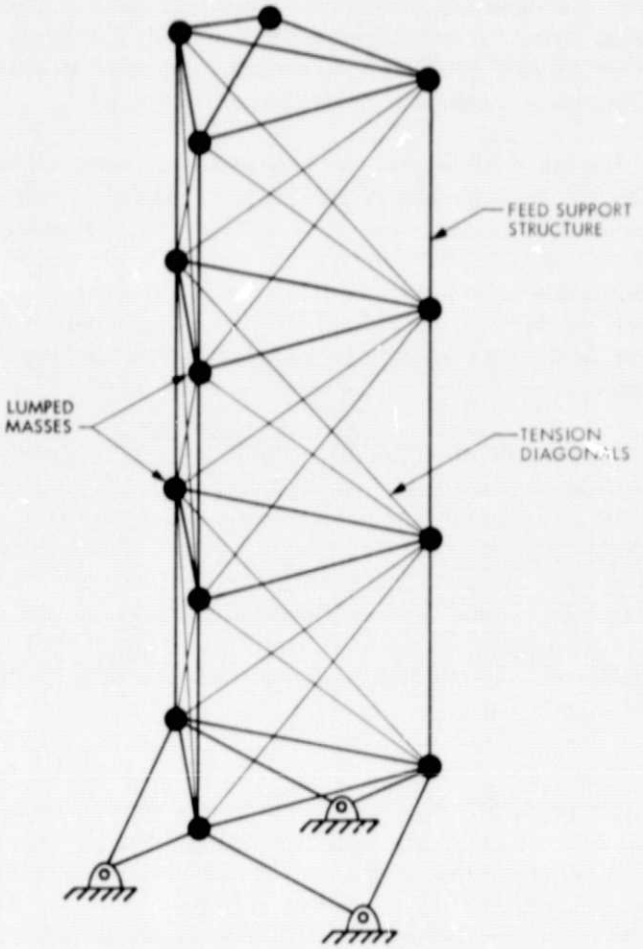

Fig. 23. Finite element model, conventional truss structure with lumped mass simulation of ribs, feed, and hub

A. Boost Configuration

The primary sources of structural loading of the antenna are the launch and boost phases of the service environment. The structural design was intended to be compatible with Mariner-class spacecraft missions which utilize Atlas/Centaur boosters. Therefore, design loading and qualification dynamic testing requirements were based on data obtained from previous Mariner programs.

As mentioned earlier, for the boost configuration, the basic load-carrying structure of the antenna is the line feed support truss. This part of the antenna supports the feed, ribs, and the entire hub including the deployment mechanism. A finite element model was developed which was representative of a conventional truss structure and accounted for the stiffness and mass distribution of the truss but only included lumped mass representations of the ribs, feed, and hub structure (Fig. 23). The development of this model was done with the SAP IV computer program (Refs. 22 and 23).

For the first iteration, member loads were based on quasistatic acceleration loading obtained from previous spacecraft programs. This was considered to be representative of worst-case loading for structures equal in mass to the antenna. The diagonals used for the truss structure are thin, elongated, flexible members and therefore can carry only tension loads (Fig. 24). To avoid compression, they were preloaded such that under the maximum expected lateral truss loading neither of the diagonals in a bay was completely unloaded. To account for this preload condition in the analysis, the truss was first analyzed with the diagonals reacting in tension and in compression to the applied lateral loading. Then, using this analysis result, the diagonals were preloaded in tension such that the same lateral loading did not produce any compression in the diagonal. Superposition of the applied lateral loading and the static loading due to the pretension in the diagonals gave the resultant member loads that were used for preliminary element sizing.

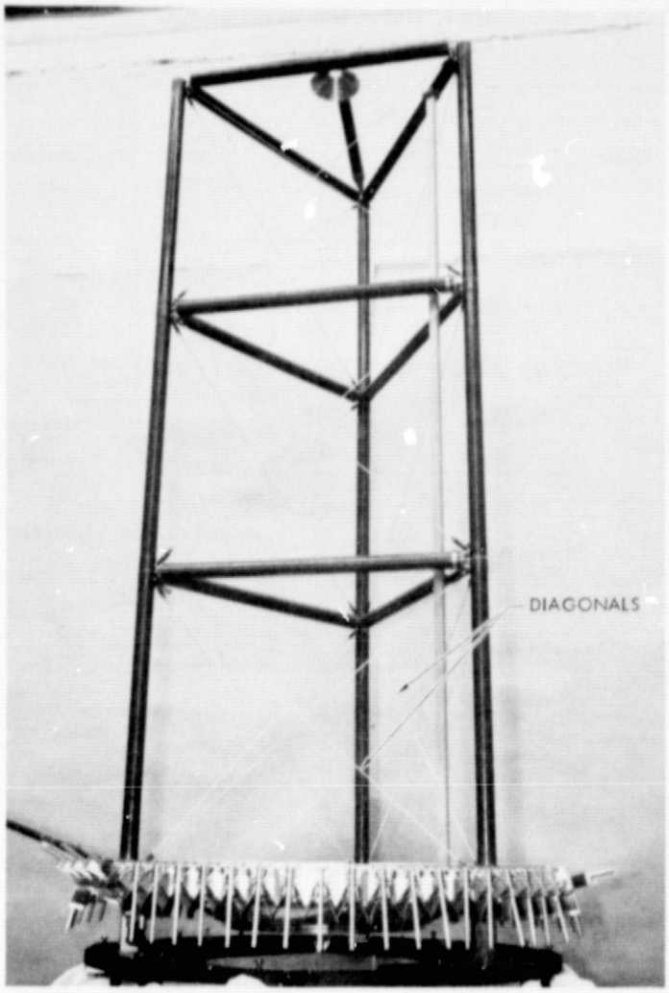

Fig. 24. Preloaded tension diagonals

Next, the natural frequencies and mode shapes were obtained with the upgraded mathematical model. This data, in conjunction with the dynamic test levels required for the antenna, was used to obtain the dynamic response loads. Then a comparison was made between the quasi-static member loads that were used for preliminary sizing and the dynamic response loads that were equivalent to qualification test levels for the antenna structure. This procedure was iterated in a traditional manner until positive structural margins of safety for all load-carrying elements of the antenna structure were obtained (Fig. 25).

B. Cruise Configuration

The finite element model developed for the cruise configuration of the structure accounted for stiffness and mass distribution of the truss, ribs, and mesh. Verification of the model was accomplished with the results of a modal survey for the configuration analyzed (Fig. 26).

Because of the inherent symmetry in the geometry of the antenna structure, only half of the deployed structure was modeled for the analysis. Two sets of such analyses were carried out: one for the antisymmetric and one for the symmetric modes by applying appropriate boundary conditions along the plane of symmetry.

In order to evaluate the possible effects of coupling between modes of the stretched reflector mesh and modes involving the deployed ribs, a special-purpose program was developed since a conventional computer program such as SAP IV does not have this capability. This program computed the frequencies and mode shapes of the

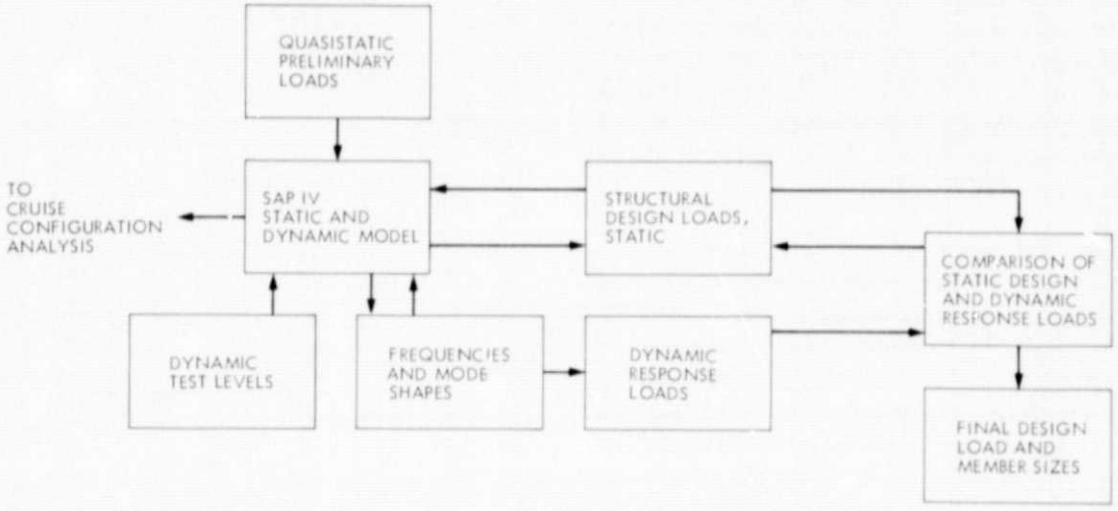

Fig. 25. Structural analysis process

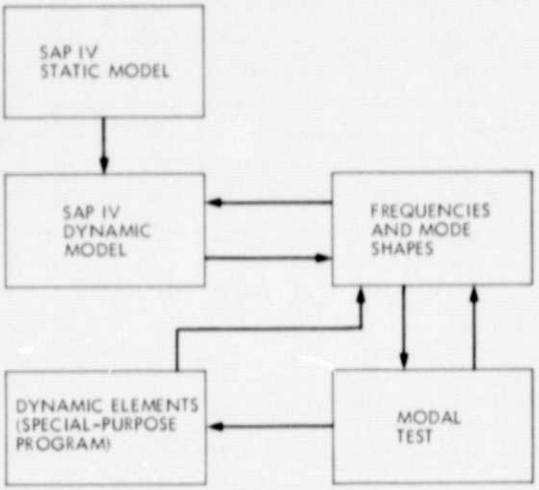

Fig. 26. Cruise configuration dynamic analysis process

tensioned mesh itself. During the development of the special-purpose program, a new finite element called "dynamic elements" was created. These elements allowed solution of this type of problem more effectively and with a fewer number of finite elements than conventional approaches. A saving in computation time by a factor of between 5 and 10 was realized, using dynamic elements in lieu of the usual finite elements. Results of the analysis indicated that the mesh frequencies were sufficiently separated from the basic structural modes to avoid coupling. A brief summary of the development is given in the Appendix.

Figure 27 is an isometric projection of half of the deployed antenna discretized by the finite element technique. Bars, beams, and membrane elements were used for the structural discretization. The SAP IV computer program was used for the final analysis. The geometric stiffness option was used to apply prestressing of the tension elements (bowstrings and spokes) before solution of the eigenproblem.

Table 4 gives the numerical results of such analysis along with the corresponding experimental data derived from the modal vibration tests mentioned in Section VI. In general, the results show excellent correlation. The test results corresponding to the first two calculated modes, which are shown within parentheses, refer to the first two computed natural frequencies of the antenna in folded configuration. The contribution of the mesh reflector to the overall stiffness of the structure was found to be minimal for this configuration.

Table 4. List of natural frequencies (deployed configuration)

Mode number	Frequencies, Hz		Nature of mode	Damping ratio
	Analysis results	Test results		
1	8.5	8.0	First torsion	0.008
2	23.7 (25.82)[a]	23.5 (25.5)[a]	Out-of-plane bending	0.015
3	24.1 (26.62)[a]	23.7 (26.0)[a]	Out-of-plane bending	0.014
4		28.7	Second torsion	
5	39.2	37.1	Out-of-plane bending	0.008
6	51.2	50.9	First plate mode	0.011
7	62.2	60.9	Second plate mode	0.010
8	63.6		Third plate mode	
9	65.91		Fourth plate mode	

[a]Furled configuration.

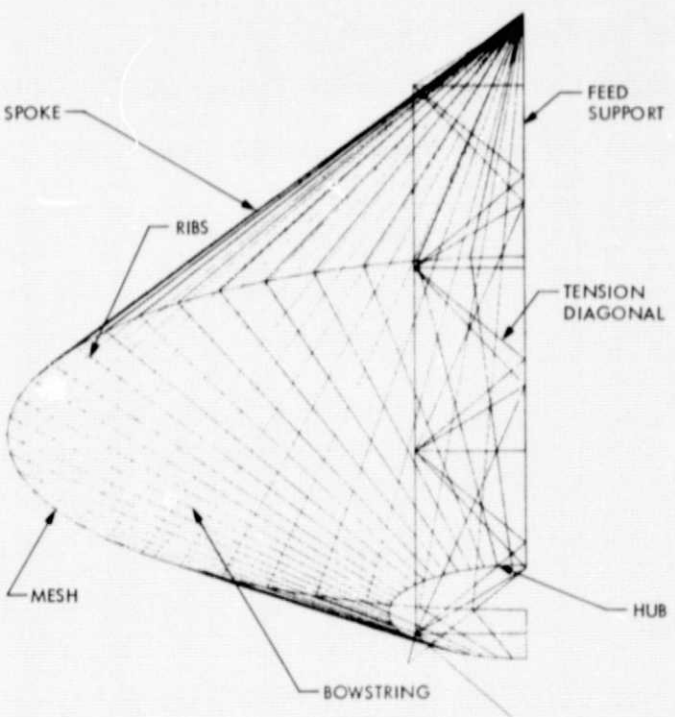

Fig. 27. Discretized model of half of deployed 5-meter conical antenna

Verification of the mathematical model of the deployed antenna was sufficient to accommodate structural/autopilot interaction analysis if required for a specific application of the antenna.

C. Thermal Considerations

Two thermal deformation mechanisms would occur during a steady-state cruise mode of a spacecraft bearing a conical antenna: those due to solar input and those due to RTG radiation.

Since most of the time the antenna will be Earth- or Sun-oriented, and since these two directions nearly coincide as viewed from the outer planets, such as Saturn, the solar input can be assumed approximately along the antenna axis and symmetrical on the front face. Solar flux filtered through the mesh will heat all the ribs uniformly and any deformation occurring will be axially symmetric. These deformations can be controlled by the length of the antenna spokes.

Flight programs currently under study for outer-planet missions configure the RTG in back of the antenna cone at a distance from the spacecraft bus. This will cause an unsymmetrical heat input which may distort the ribs closest to it. Using the Mariner/Jupiter Saturn 1977 spacecraft configuration to represent the relative locations of the antenna and RTG, a first approximation of rib heating was obtained by assuming a point source of 8100 watts at a distance of 2 meters from the center of the rib and at an angle of approximately 45 deg from the vertical to the surface (Fig. 28).

For a location near Saturn, the mesh forming the cone surface, made from silver-coated wire, would stabilize at approximately 100 K, the equilibrium temperature due to the solar energy flux. Superimposing the 8100-W unsymmetric RTG radiation heating would locally raise the mesh temperature to 154 K, while the opposite side of the dish, because of shading and a near zero view factor, would remain at 100 K. Thus, going around the antenna surface, the maximum temperature difference is 54 K with an approximately linear temperature distribution. Since the bowstrings are in contact with the mesh, they would be approximately the same temperature. The spokes, however, would increase in temperature to 112–116 K.

The rib equilibrium temperature at Saturn distances as obtained by applying an 0.8 filter factor to the local solar intensity was calculated to be about 93 K. The variance in rib temperature would be about 54 K as in the case of the antenna surface, for a maximum of 147 K.

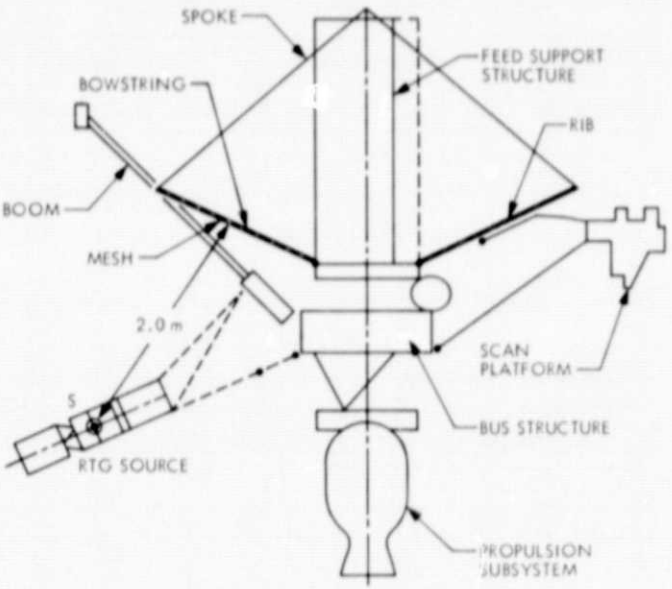

Fig. 28. Mariner/Jupiter Saturn 1977 spacecraft configuration with deployed 5-meter conical antenna

Thermal distortion was examined as a function of structural material. As an example, absorption of the infrared energy on one side of an aluminum rib would cause bending in an arc convex toward the heat source and with it a reduction of the length (distance between end points of the rib). This bending varies inversely as the thermal conductance around the tube. In the case of a high thermal conductance of the rib material, uniform distribution around the tube of the absorbed IR energy would expand the rib but not bend it. Graphite epoxy ribs have a low thermal conductivity, but they can be fabricated in a form in which the effective coefficient of thermal expansion is very nearly zero. This property eliminates bending due to thermal gradients in the ribs and thus minimizes thermal distortion.

Overall thermal distortion of the antenna structure can be expressed in terms of changes of member length and in the conical reflector half-angle, nominally 65 deg. Two classes of contributions were considered (Table 5):

(1) Shrinkage of the whole structure due to transfer of the antenna from an Earth environment to a Saturn space location.

(2) Differential angular changes of the two sides of the cone due to unsymmetrical RTG heating.

Table 5. Overall antenna thermal distortion

Antenna	Earth/Saturn transfer			RTG effect		
Component	mm	(in.)	deg.	mm	(in.)	deg.
Ribs	−0.76	(−0.030)	+0.010	−0.20	(+0.008)	−0.003
Spokes	−1.17	(−0.046)	−0.035	−0.025	(−0.001)	+0.001
Feed supports	−1.27	(−0.050)	+0.025	+0.025	(+0.001)	−0.000
Total effect			<−0.001			−0.002

The total change of the cone half-angle is then about −0.003 deg, a small closing motion of the antenna cone. It is noteworthy that most of the thermal distortions compensate each other, especially the common shrinking of the feed support and spokes, resulting in a small net angle change, even though large temperature changes occur during planetary transfer. In the vicinity of Saturn, the unsymmetric RTG heating causes approximately two and a half times the distortion due to planetary transfer.

VI. Antenna Test Program

The furlable antenna test program was intended to evaluate and demonstrate the mechanical, structural, and RF functional properties of the flight-type hardware. The test program was initiated with reflector surface measurement and adjustment and was followed by multiple furling and unfurling of the ribs to determine the repeatability of the reflecting surface quality. The next phase was an RF range test at 8.5 GHz to measure the RF gain patterns and overall operating efficiency. Structural evaluation of the antenna was accomplished by a modal vibration test to verify the finite element mathematical model of the antenna hardware. The modal test was accomplished for both the boost and cruise configurations. Natural frequencies and mode shapes were obtained for the line feed support structure and the antenna reflector support structure.

A. Surface Evaluation

Because the antenna RF performance is strongly influenced by the accuracy of the reflecting surface, it is necessary to know the surface accuracy of the conical reflector so that gain loss can be estimated. It is also desirable to make the surface measurement with the antenna in the same position or attitude as for the RF test.

At the JPL antenna test range, RF testing was performed with the axis of the antenna horizontal. This resulted in an unsymmetrical gravity field on the reflecting surface applied perpendicular to its axis of symmetry. This gravity load caused the reflecting surface above the antenna axis to deflect toward the antenna axis. The reflecting surface below the antenna axis deflected away from the antenna axis. To include these effects, the surface deviation of the conical mesh reflector was measured with the cone axis horizontal, as it would be during RF testing.

The technique used to measure the deviation of the mesh conical surface is similar to that of Ref. 9 and is indicated in Fig. 29. The tubular triangular support truss provided the interface between a handling fixture and a bearing plate attached to the three antenna support points. A precision track, parallel to the theoretically

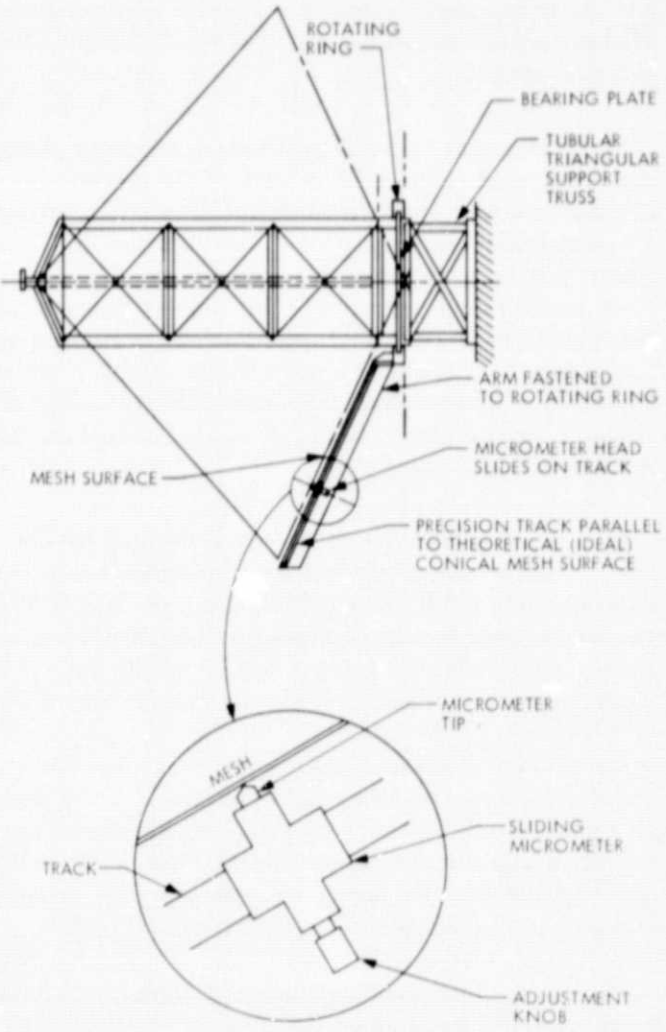

Fig. 29. Surface evaluation test setup in horizontal position

perfect conical surface, was attached to a rotating ring and generated an "ideal" conical surface when rotated about the antenna axis. A micrometer head was attached to a radially movable mount on the track. Thus, any point on the reflector surface could be measured by rotation of the track and radial movement of the micrometer. The flexibility of the mesh presented a problem in sensing where the micrometer touched the mesh. To sense the contact, shiny foil discs, 16 mm (0.62 in.) in diameter, were attached to the mesh. The position of the mesh surface was established when the micrometer spindle tip appeared to just touch its reflection in the shiny disc.

To avoid the obvious interference of the spokes and bowstrings and to minimize costs, the evaluation of the mesh surface was accomplished from the rear, as opposed to the evaluation of Ref. 9, which was done from the front. The rear surface technique was more difficult. As an example, the mesh surface approximates a conical reflector by forming a 60-sided pyramid; i.e., 60 panels and 60 ribs. A true rms measurement would include the values at the centerline and edge of each panel. However, no measurements were made within 5.08 cm (2 in.) of a panel corner because of rib interference. This interference resulted in a more limited sampling of measuring points. Five measuring points per panel were established (Fig. 30), leading to a total of 300 measurements for the entire reflector.

The rms value of the surface deviation Δ was computed by

$$\Delta = \sqrt{\frac{\sum_{i}^{n} (\delta_i - \delta)^2}{n}}, \quad \delta = \frac{1}{n}\sum_{i}^{n} \delta_i$$

where

δ_i = measured deviations of the surface from the rotating track

n = number of measurements

Based on the 300 measurements, the Δ of the reflector was computed to be 0.61 mm (0.024 in.) rms. This is to be compared to the computed surface accuracy of a theoretically perfect 60-sided pyramid, 0.43 mm (0.017 in.) rms. However, a portion of the difference between the actual and theoretical can be attributed to tolerances in the rotating track mechanism and eccentricity of the bearing plate, estimated at ± 0.10 mm (± 0.004 in.).

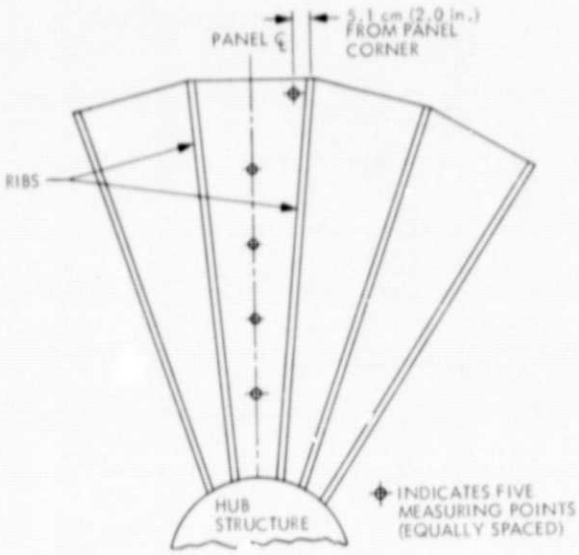

Fig. 30. Measurement points on typical mesh panel of 5-meter conical antenna

B. RF Test Range

A series of RF tests were made on the antenna at the JPL test range (Fig. 31). Antenna amplitude pattern, phase, and gain were measured with the aid of an illumination antenna and transmitter that were located 1006 m (3300 ft) downrange from the antenna. The illumination antenna had a narrow bandwidth to minimize the effects of ground reflections. The 5-meter antenna was mounted on a rotating fixture to accommodate the boresight angle changes required to implement the RF range test. Variation of azimuth, to change the boresight angle of the antenna while holding constant elevation, provided the patterns, while absolute gain was obtained by comparison with the gain of a standard calibrated antenna located adjacent to the conical antenna.

To prevent wind-induced deformation of the antenna reflecting surface during RF test, an inflatable radome was used to provide a protection shield around the antenna (Fig. 32). The radome was made of dacron material cut and sewed into the required geometric dome shape. Stiffness was obtained by air pressure. RF testing of the 5-meter antenna with and without the radome on a very calm day indicated that the RF loss associated with the dacron was less than 0.10 dB.

The mesh corrosion problems previously mentioned necessitated the implementation of a large series of RF tests. These RF range tests were repeated after several

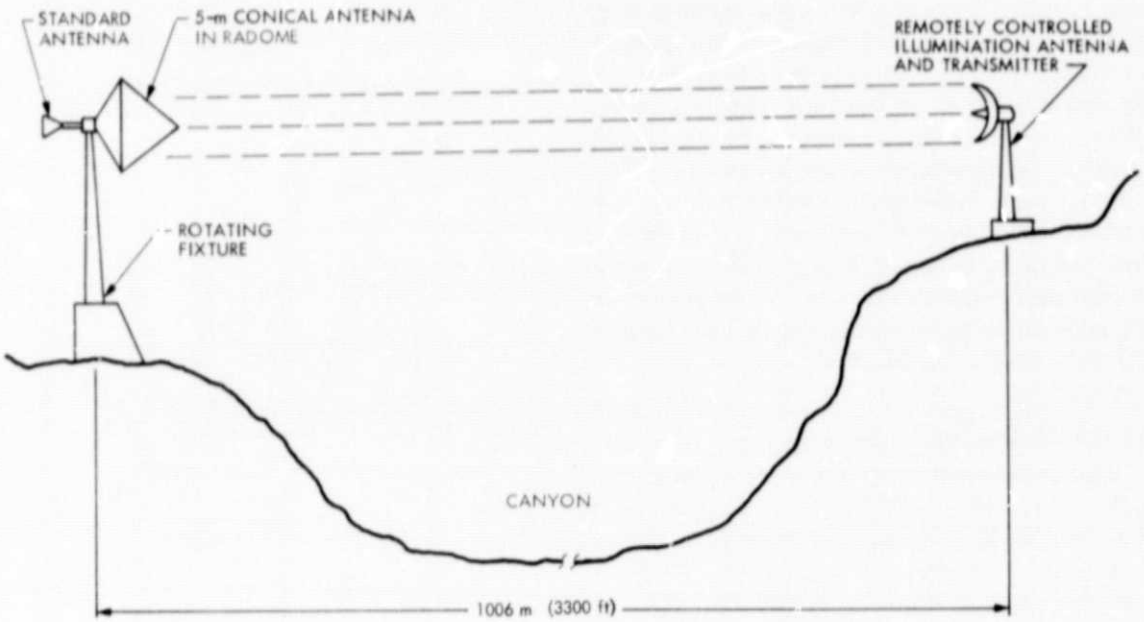

Fig. 31. RF test range for 5-m conical antenna

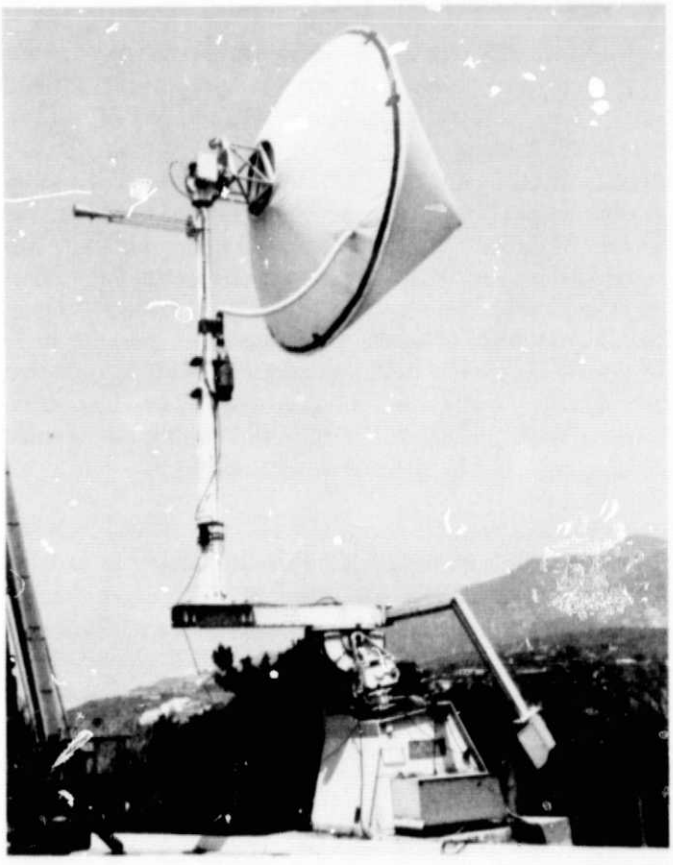

Fig. 32. RF testing of 5-meter conical antenna equipped with inflatable dacron radome

attempts to chemically remove the corrosion from the mesh, until the electrical performance was considered to be optimum for the deteriorated condition of the mesh. The best RF performance was 49.77 dB at 8.5 GHz for an overall efficiency of the input to the line source feed of 53.0%. It is anticipated that the design goal of 55% efficiency could have been exceeded had the mesh RF reflectivity remained good, since the small surface deviation of the reflector was commensurate with a high-performance furlable antenna.

C. Modal Test

The objective of the modal test was to identify natural frequencies and measure the associated mode shapes for comparison with the properties of the structural mathematical model of the antenna. The antenna structure was cantilever-mounted at its base for both the furled and deployed test configuration (Figs. 33 and 34).

Sinusoidal excitation was provided by electromagnetic shakers that utilized very small armature masses to minimize their effect on the frequency and mode shapes of the test structure. A total of six shakers operating at the same frequency and exactly in phase or out of phase with respect to each other were used to adequately excite the modes. Dynamic mode shapes were measured with the use of piezoelectric accelerometers. Accelerometers were permanently mounted on structure not easily accessible during the test, such as the line feed support structure.

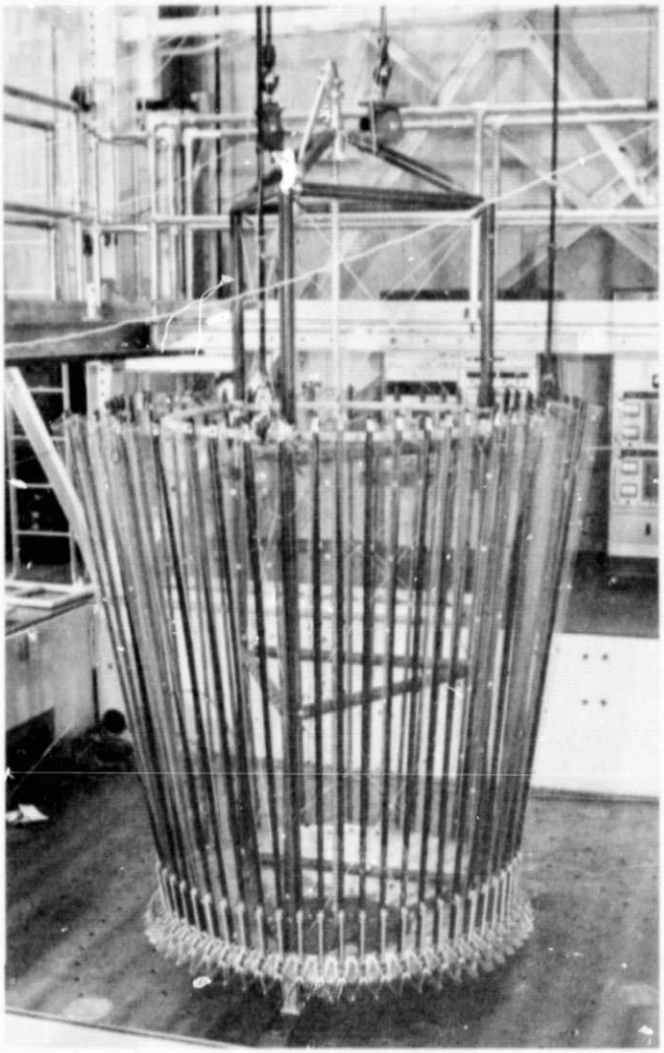

Fig. 33. Modal test setup for 5-meter conical antenna, furled configuration

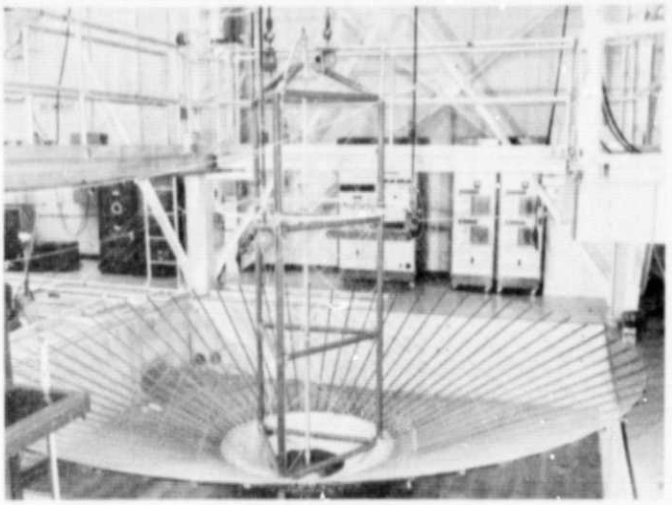

Fig. 34. Modal test setup for 5-meter conical antenna, deployed configuration

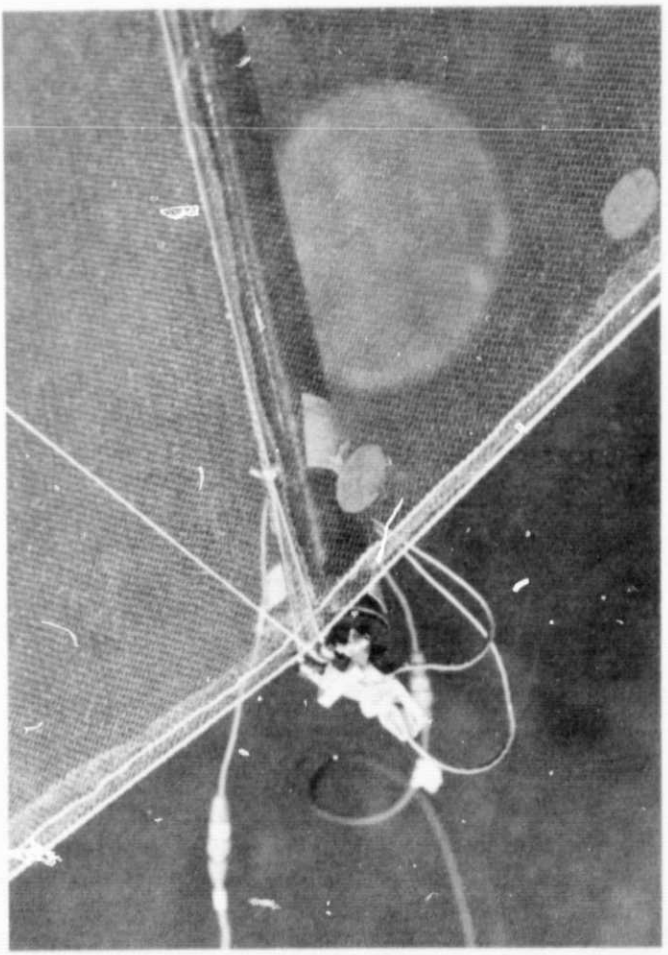

Fig. 35. Measurement of rib tip motion with portable accelerometer

Otherwise, dynamic motion was measured with a portable accelerometer, e.g., motion of the deployed rib tips (Fig. 35).

The lowest frequency mode of the deployed structure was first torsion, at 8.0 Hz. The ribs accounted for essentially all of the motion while the line feed support structure amplitude was too low to be measured. The ribs deformed in bending, similar to a series of cantilever beams, attached to each other by the mesh, symmetrically about the antenna axis. The fundamental bending modes of the line feed support structure, 23.5 and 23.7 Hz, respectively, for the unfurled configuration were easy to excite and isolate with two shakers. These modes were similar in shape to the first cantilever mode of a uniform

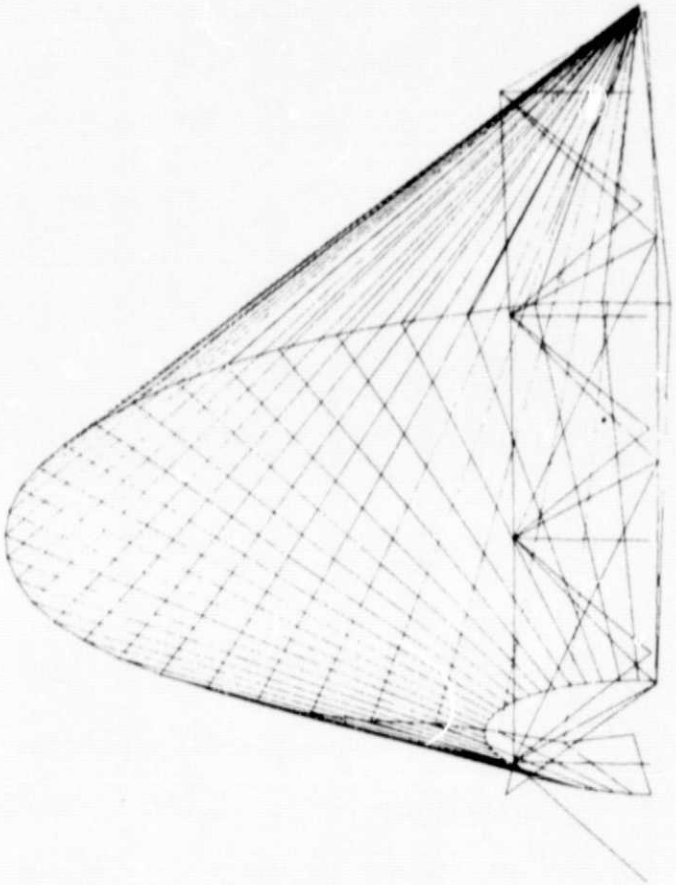

Fig. 36. Fundamental mode of feed support structure, bending at 23.7 Hz

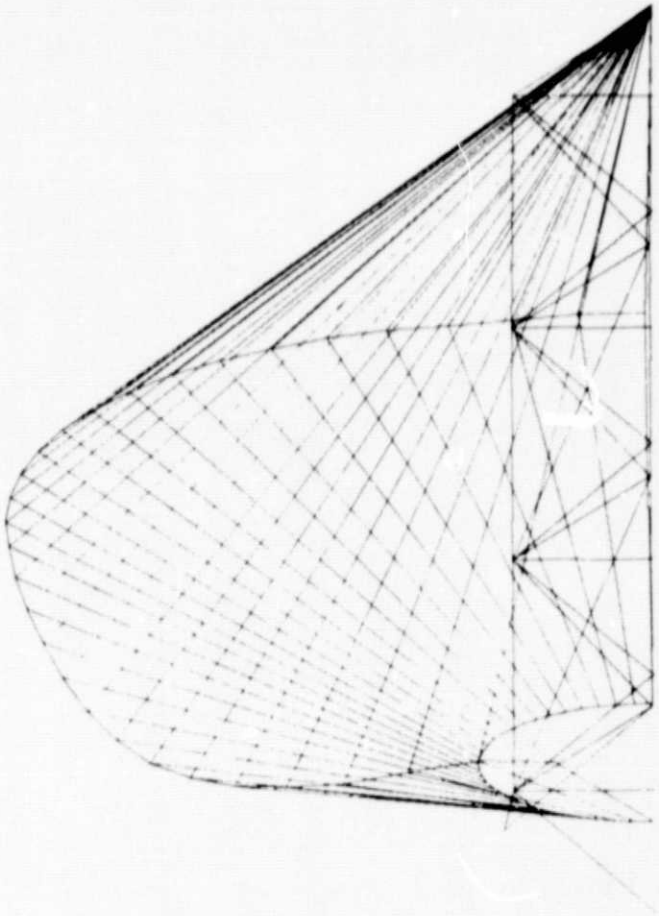

Fig. 37. Fundamental reflector mode, classical circular plate edges rocking at 50.9 Hz

beam (Fig. 36). However, the second bending mode, 37.1 Hz, required the use of four shakers. Again, this mode was somewhat equivalent to the second mode of a cantilevered beam. The first elastic mode of the reflector structure, 50.9 Hz, required excitation of the line feed support structure and the tips of several ribs. However, the ribs and mesh accounted for the maximum dynamic displacement, while the line feed support structure barely participated in the mode. The deflected shape of the ribs and mesh (Figure 37) was similar to a fundamental classical circular plate mode where the edges rock about an axis of symmetry.

Estimates of structural damping for each mode mapped were determined from acceleration decay traces that were obtained by terminating forced response and recording the accelerometer output. These damping values varied from 0.008 to 0.0015. See Table 4 for a summary of test results.

VII. Assessment of Antenna Program Results

The experience derived from the concept and hardware development program has led to certain conclusions and opinions as to how the 5-meter antenna compares to state-of-the-art furlable antenna technology.

The 5-meter antenna has several advantages when compared to other furlable antennas that have either been built and tested or have been built, evaluated and flown as part of flight projects. The cost of fabrication and surface adjustment of the conical antenna is considerably less because high-tolerance parts are not required and surface adjustment after assembly is simple and quick to accomplish. The surface tolerance of the 5-meter antenna is about as good as any other antenna design that has been demonstrated by flight-type hardware. The deployed natural frequencies are so high that structural/autopilot coupling would not be a problem for virtually any flight

applications. Additionally, the structural stiffness leading to the high natural frequencies would allow moderate scanning rates without significant deformation of the reflecting surface. The basic configuration of the conical antenna, along with the materials used for construction, results in an excellent thermal design. Because of the relative insensitivity of the reflecting surface to small changes in bowstring tension, overall temperature changes, and thermal gradients, reflector surface distortions are very small. Other concepts that are dependent on purely cantilevered rib configurations are much more sensitive to temperature changes and gradients.

Limitations associated with the conical antenna as compared to state-of-the-art designs include single-frequency operation for the line source feed, antenna weight, and mechanical packaging efficiency. Current technology limits the use of the line source feed to only one frequency for efficient operation. Dual-frequency operation of the line source feed has been demonstrated, i.e., S- and X-band, but with significantly reduced RF efficiency. The 5-meter antenna is heavier than most other designs, but for a flight application the weight could be reduced by optimizing fittings and member sizes to be compatible with some of the other furlable antennas. The mechanical packaging of the 5-meter antenna is limited by the length of the ribs, line source feed, and the diameter of the line feed support structure. Its packaging efficiency is roughly equivalent to other furlable antennas with folding ribs, but considerably less than designs utilizing wrap ribs or truss members.

Current deep space mission studies at JPL have considered the use of single-frequency high-data-rate antennas operating at X-band. For applications of this type for the 5-meter antenna, only minor changes to the design would be required. These would include simplification of the deployment mechanism, reduction of weight by about 25%, and a surface treatment or coating to the reflector mesh to eliminate the corrosion problem.

An overall assessment of the 5-meter antenna indicates that the advantages of the design demonstrated warrants further development of the line source feed for a dual-frequency capability.

VIII. Results and Conclusions

The concept of a flight-type conical reflector antenna with a line source feed was functionally demonstrated. The design criteria established for the antenna were closely matched as indicated in Table 6.

In addition to successfully meeting these criteria, the following results are noteworthy:

(1) Automated deployment and furling with controlled rates was achieved.

(2) The application of structural composites to obtain high stiffness-to-weight, thermal stability, and RF transparency was demonstrated.

(3) New structural analysis capability applicable to other types of antennas was developed.

(4) The corrosion problems associated with the silver-plated beryllium copper mesh probably accounted for the degraded RF performance. A solution to the mesh corrosion problem was developed. Long-range solutions remain to be found.

In conclusion, a very large amount of experience was gained through the development of the 5-meter antenna. This experience is directly applicable to other, current JPL antenna development programs.

Table 6. Comparison of design criteria with actual results

Design condition	Criteria	Actual
Physical		
Furled diameter	1.5 m	1.5 m
Furled length	4 m	4 m
Deployed diameter	5 m	5 m
Mass	37 kg	32 kg
Surface tolerance	0.64 mm rms	0.61 mm rms
Feed alignment	±0.2 cm (Translational) 0.01 radian	
Electrical		
Frequency	X-band	X-band (8.5 Ghz)
Operating efficiency	55%	53%
Gain	49.8 dB	49.77 dB
Feed	Line source	Line source
Environmental		
Structural loads	Launch/deployment	Confirmed by analysis and test
Natural frequency	≥0.1 Hz deployed ≥ 12 Hz furled	8.0 Hz 25.5 Hz
Thermal	33 to 367 K	Confirmed by analysis

Appendix

Development of the Finite Dynamic Element Method

During the modeling of the antenna mesh reflector it was noted that the conventional finite element modeling would yield a rather large number of algebraic equations, resulting in a rather expensive eigenproblem solution process. The concept of the newly developed dynamic element method (DEM) was developed in the search for an alternative, economical procedure for structural discretization. The capability now exists to efficiently and economically determine the dynamic properties of membrane structural elements that are characterized by lateral natural frequencies varying as a function of in-plane stress. In addition, the concept of dynamic elements can be readily extended to other finite elements such as the plate bending and shell elements. This would facilitate dynamic solution with improved accuracy and a reduced number of finite elements as compared to conventional approaches.

The finite element method is characterized by the fundamental relationship

$$\mathbf{u} = \mathbf{aU} \tag{A-1}$$

which defines the continuous displacement vector within an element in terms of its unknown nodal displacement parameters. This relationship is only valid for static loading, since for free and forced harmonic motion **a** is not only a function of instantaneous element nodal displacements but also of the frequency ω of such motion; the resulting stiffness and inertia matrices are then obtained as functions of ω. The extraction of roots from the initially unknown frequency-dependent matrices is prohibitively expensive for most practical problems. Thus the matrix **a** is expressed in series form in ascending powers of ω:

$$\mathbf{a} = \sum_{r=0}^{\infty} \omega^r \mathbf{a}_r \tag{A-2}$$

when the stiffness and inertia matrices are obtained as follows:

$$\mathbf{K} = \mathbf{K}_0 + \omega^2\mathbf{K}_2 + \omega^4\mathbf{K}_4 + \cdots \tag{A-3}$$

$$\mathbf{M} = \mathbf{M}_0 + \omega^2\mathbf{M}_2 + \omega^4\mathbf{M}_4 + \cdots \tag{A-4}$$

which results in the equation of motion

$$[\mathbf{K}_0 - \omega^2(\mathbf{M}_0 - \mathbf{K}_2) - \omega^4(\mathbf{M}_2 - \mathbf{K}_4) - \cdots]\mathbf{q} = \mathbf{O} \tag{A-5}$$

q being the amplitudes of **U**, and $\mathbf{M}_0$, $\mathbf{K}_0$ the static inertia and stiffness matrices, while the higher-order terms constitute the dynamic corrections. Usual free vibration analysis of structures involves the static matrices only, the procedure being identified as the well-known finite element method (FEM).

The equation of motion for such a case is given by

$$\mathbf{M}_0\mathbf{q} + \mathbf{K}_0\mathbf{q} = \mathbf{O} \tag{A-6}$$

which results in the usual eigenvalue problem

$$(\mathbf{K}_0 - \omega^2\mathbf{M}_0)\mathbf{q} = \mathbf{O} \tag{A-7}$$

when it may be recognized as a special case of the more general eigenvalue problem defined by Eq. (A-5). Inclusion of the dynamic correction terms results in the quadratic matric eigenvalue problem (Eq. A-5), the solution of which effects most significant improvements in root convergence (Refs. 24 and 25). The procedure is termed the dynamic element method (Ref. 26) and such dynamic correction matrices have been developed for a rectangular membrane element (Fig. A-1). Figures A-2 and A-3 present the relative efficiency of the FEM and DEM techniques when it may be observed that the DEM solution is about an order of magnitude faster than the usual FEM analysis. Full details of this new development are given in Ref. 26.

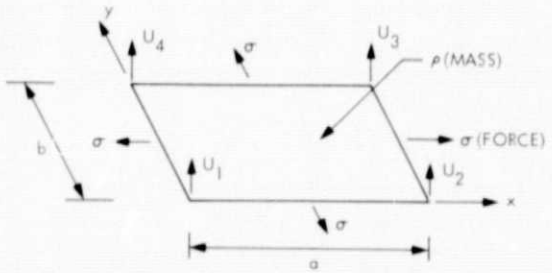

Fig. A-1. Rectangular membrane element

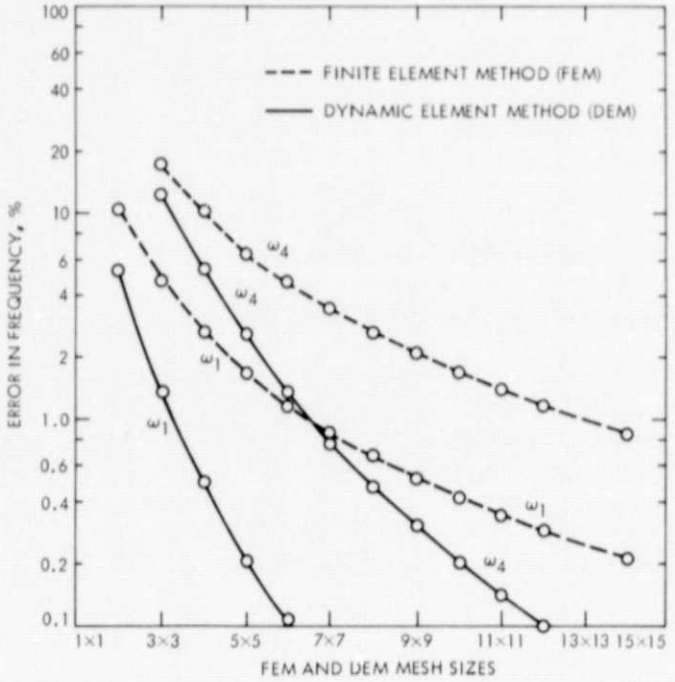

Fig. A-2. Comparison of convergence characteristics of FEM and DEM

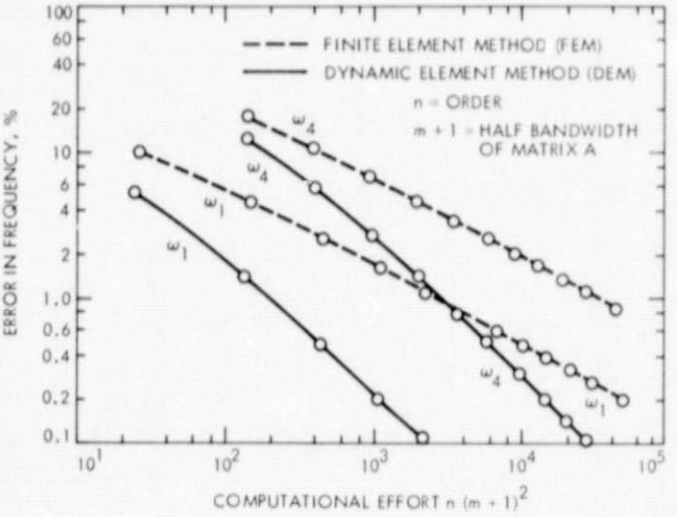

Fig. A-3. Comparison of computational effort for FEM and DEM

References

1. Freeland, R. E., Smith, J. G., Springett, J. C., Woo, K. E., "Large Deployable Antenna Shuttle Experiment," Paper No. AAS 75-253, presented at the American Astronautical Society 21st Annual Meeting, Denver, Colo., August 26–28, 1975.

2. Fisher, J. G., "Development of a Conical-Gregorian High Gain Antenna," in *Supporting Research and Advanced Development*, Space Programs Summary 37-63, Vol. III, pp. 124–128, Jet Propulsion Laboratory, Pasadena, Calif., June 30, 1970.

3. Fisher, J. G., "Mesh Materials for Deployable Antennas," in *Supporting Research and Advanced Development*, Space Programs Summary 37-65, Vol. III, pp. 122–125, Jet Propulsion Laboratory, Pasadena, Calif., Oct. 31, 1970.

4. Ludwig, A. C., Woo, K., Gustincic, J. J., and Hardy, J. C., "Recent Development of Conical Reflector Antennas," paper presented at the IEEE International Symposium, Boulder, Colo., Aug., 1973.

5. Ludwig, A. C., "Large Spacecraft Antennas (Non-Paraboloidal Reflector)," in *Supporting Research and Advanced Development*, Space Programs Summary 37-59, Vol. III, pp. 55–57, Jet Propulsion Laboratory, Pasadena, Calif., Oct. 31, 1969.

6. Ludwig, A. C., and Hardy, J., "Preliminary RF Test of Conical Gregorian Antenna," Space Programs Summary 37-63, Vol. III, pp. 42–45, Jet Propulsion Laboratory, Pasadena, Calif., June 30, 1970.

7. Ludwig, A. C., "A New Geometry for Unfurlable Antennas," *Microwaves*, Nov. 1970.

8. Ludwig, A. C., "Conical Reflector Antennas," *IEEE Trans.*, Vol. AP-20, No. 2, Mar. 1972.

9. Moore, D. M., *Lightweight 3.66-Meter-Diameter Conical Mesh Antenna Reflector*, Technical Memorandum 33-685, Jet Propulsion Laboratory, Pasadena, Calif., June 15, 1974.

10. Oliver, R. E., "Large Spacecraft Antennas: New Geometric Configuration Design Concepts," in *JPL Quarterly Technical Review*, Vol. 1, No. 1, pp. 78–85, Jet Propulsion Laboratory, Pasadena, Calif., Apr. 1971.

11. Oliver, R. E., and Wilson, A. H., *Furlable Spacecraft Antenna Development: An Interim Report*, Technical Memorandum 33-537, Jet Propulsion Laboratory, Pasadena, Calif., Apr. 15, 1972.

12. Oliver, R. E., Trubert, M. R., and Wilson, A. H., "Large Spacecraft Antennas: Conical Ring-Membrane Reflectors," in *JPL Quarterly Technical Review*, Vol. 2, No. 2, pp. 41–47, Jet Propulsion Laboratory, Pasadena, Calif., July 1972.

13. Oliver, R. E., and Wilson, A. H., *Furlable Spacecraft Antenna Development: Second Interim Report*, Technical Memorandum 33-606, Jet Propulsion Laboratory, Pasadena, Calif., May 15, 1973.

14. Robinson, E. Y., Stonier, R. A., and Lofgren, C. L., "Development of a Unique Graphite/Epoxy Antenna Component," paper presented at the Third Annual Conference on Composite Materials: Testing and Design, ASTM, Williamsburg, Va., Mar. 1973.

15. Woo, K., and Otoshi, T. Y., "Spacecraft Antenna Research. An RF Study of Reflector Surface Materials for Spacecraft Antennas," in *Supporting Research and Advanced Development*, Space Programs Summary 37-61, Vol. III, pp. 99–106, Jet Propulsion Laboratory, Pasadena, Calif., Feb. 28, 1970.

16. Cramer, P. C., "Conical Quadreflex Antenna Analytical Study," Technical Report 32-1591, Jet Propulsion Laboratory, Pasadena, Calif., Dec. 15, 1973.

17. Bright, T., Every, R., Sheppard, R., and Manson, R., "Systems Impact of a Conical Antenna for Planetary Communications," Preprint No. AAS-71-151, presented at the American Astronautical Society 17th Annual Meeting, Seattle, Wash., June 29–30, 1971.

18. Clevett, M. L., (Martin Marietta Corp.), "Conical Antenna Design Concepts," intracompany design study report, May 1971.

19. Ruze, J., "Antenna Tolerance Theory—A Review," *Proc. IEEE*, Vol. 54, No. 4, April 1966, pp. 633-640.

20. Bogner, F. K., "Analysis of Tension Structures," *Proceedings of the Second Conference on Matrix Methods in Structural Mechanics*, Air Force Dynamics Laboratory, Wright-Patterson AFB, Dayton, Ohio, AFFDL-TR-68-150, Oct. 1968, pp. 1253–1271.

21. Levy, Donald J., and Momyer, William R., "Advanced Antenna Meshes for Spacecraft Unfurlable Reflectors," LMSC/D407132, Lockheed Palo Alto Research Laboratory, Palo Alto, Calif., June 15, 1972.

22. Wilson, E. L., et al., "A Structural Analysis Program for Static and Dynamic Response of Linear Systems," Report No. EERC 73-11, University of California, Berkeley, June 1973.

23. Norton, R. L., "Implementation and Use of the Geometric Stiffness Matrix for Plate and Beam Elements in SAP IV," paper to be presented at the First SAP Users Conference and Computer Workshop, June 7–11, 1976, University of Southern California, Department of Civil Engineering, Los Angeles, Calif.

24. Gupta, K. K., "Solution of Quadratic Matrix Equations for Free Vibration Analysis of Structures," *Int. J. Num. Meth. Eng.*, Vol. 6, 129–135, 1973.

25. Gupta, K. K., "Numerical Solution of Quadratic Matrix Equations for the Dynamic Analysis of Structures," *Computational Aspects of Finite Element Method*, proceedings of symposium held at Imperial College, London, Sep. 1975.

26. Gupta, K. K., "On a Finite Dynamic Element Method for Free Vibration Analysis of Structures," *Comp. Meth. Appl. Mech. Eng.*, Vol. 8, No. 1, 1976.

NASA—JPL—Coml., L.A., Calif.